

A review of the Magnus effect in aeronautics

Jost Seifert*

EADS Cassidian Air Systems, Technology and Innovation Management, MEI, Rechliner Str., 85077 Manching, Germany

ARTICLE INFO

Available online 14 September 2012

Keywords:

Magnus effect
Rotating cylinder
Flettner-rotor
Rotor airplane
Boundary layer control

ABSTRACT

The Magnus effect is well-known for its influence on the flight path of a spinning ball. Besides ball games, the method of producing a lift force by spinning a body of revolution in cross-flow was not used in any kind of commercial application until the year 1924, when Anton Flettner invented and built the first rotor ship *Buckau*. This sailboat extracted its propulsive force from the airflow around two large rotating cylinders. It attracted attention wherever it was presented to the public and inspired scientists and engineers to use a rotating cylinder as a lifting device for aircraft. This article reviews the application of Magnus effect devices and concepts in aeronautics that have been investigated by various researchers and concludes with discussions on future challenges in their application.

© 2012 Elsevier Ltd. All rights reserved.

Contents

1. Introduction	18
1.1. History	18
1.2. Magnus force	20
1.3. Ideas and visions	21
1.3.1. Driving a Magnus rotor	21
1.3.2. Combination of different lifting devices	21
1.3.3. Enhancing the Magnus effect	22
2. Physics of flight	23
2.1. Aerodynamics of a rotating body in cross-flow	23
2.1.1. Definition of forces and moment	23
2.1.2. Effect of velocity ratio	23
2.1.3. Negative Magnus force	24
2.1.4. Autorotation	24
2.1.5. Effect of Reynolds number	25
2.1.6. Effect of surface roughness	25
2.1.7. Effect of aspect ratio	26
2.1.8. Effect of rounded ends	26
2.1.9. Effect of disks	27
2.1.10. Summary of aerodynamic coefficients	28
2.2. Gyroscopic forces on a Magnus rotor	29
3. Applications	30
3.1. Ships	30
3.1.1. Rotor ship <i>Buckau</i>	30
3.1.2. rotor ship <i>Barbara</i>	31
3.2. Aircraft	32
3.2.1. Rotor airplanes	32
3.2.2. Autogyro of Chappedelaine	33

Abbreviations: AoA, Angle of Attack; DOC, Direct Operating Costs; MAV, Micro Aerial Vehicle; MRO, Maintenance, Repair and Overhaul; MSBC, Moving Surface Boundary Layer Control; MTOW, Maximum Take Off Weight; OWE, Operating Weight Empty; RPM, Revolutions Per Minute; URANS, Unsteady Reynolds-Averaged Navier-Stokes; STOL, Short Take Off and Landing; VTOL, Vertical Take Off and Landing

*Tel.: +49 8459 8181704; fax: +49 8459 8180647.

E-mail addresses: jost.seifert@gmx.net, jost.seifert@cassidian.com

3.2.3.	Test aircraft NASA YOY-10.	33
3.2.4.	Lighter-than-air system	34
3.3.	Magnus effect devices	35
3.3.1.	Boundary layer control by a rotating cylinder integrated in an airfoil	35
3.3.2.	Vortex flap	39
3.3.3.	Propulsion.	39
3.3.4.	Hybrid rotor	39
4.	Discussion and summary.	40
4.1.	Comparison between wing and rotating cylinder.	40
4.1.1.	Stall characteristics	41
4.1.2.	Gust sensitivity in longitudinal motion.	41
4.2.	Recommendations for aircraft conceptual design.	41
4.3.	Stability and control of a rotor airplane	42
5.	Conclusions and outlook	43
	Acknowledgements	43
	Appendix A. Supplementary material	43
	References	43

1. Introduction

Very few devices based on the Magnus effect have attracted attention or were crowned by success. On the other hand, its potential benefit compared to other airfoil-based lifting devices, such as a high lift coefficient, inspired engineers to develop devices for extracting wind energy, to propel and to steer vessels and ultimately to lift an airplane. Many research results on rotating cylinders were presented in the literature which focus mainly on the generation of aerodynamic forces. To review Magnus effect applications in aeronautics, the scientific literature is surveyed in this paper as well as newspaper articles and patent specifications in order to illustrate the whole context.

In this paper the Magnus effect is defined as a device that provides a moving wall on its body to influence the boundary layer around the device, in order to produce a lifting force perpendicular to the flow direction. A rotor airplane is defined as an airplane which uses the Magnus effect for lift generation. Similar devices which generate a lifting force due to blowing or suction are not taken into account here (e.g., the Alcyone of Jacques Cousteau using Turbosails). Many ideas are published in the literature on how to use the Magnus effect in naval or aeronautical applications. Only a few ideas led to innovations. In this paper a brief history of Magnus effect research is presented, followed by a discussion of ideas and concepts for the required propulsion of a Magnus rotor, for a combination of different lifting devices, and for an enhancement of the Magnus effect. Details on the flight physics of a Magnus rotor are given and the aerodynamic characteristics and gyroscopic effects are highlighted. Successes and failures in the application of Magnus effect devices in aeronautics are discussed. A few examples of full size rotor ships and rotor airplanes are presented, to point out that there are still technology gaps to overcome. This is followed by a discussion of aircraft conceptual design and stability and control aspects. Finally the unique characteristics of a Magnus effect device are discussed which offer operational advantages for an airplane and therefore may justify the design of a new rotor airplane configuration. Concluding remarks on recent advances in Magnus rotor technology in the modern day context complete this review.

1.1. History

Isaac Newton is said to have been the first to explain the motion of a tennis ball in relation to its spin. In his letter to Oldenburg in 1671, writing about the dispersion of light, he explained “I remembered that I had often seen a tennis ball

struck with an oblique racket describe such a curved line. For a circular as well as progressive motion being communicated to it by that stroke, its parts on that side where the motions conspire must press and beat the contiguous air more violently, and there excite a reluctance and reaction of the air proportionately greater” [1,2].

At the beginning of the 19th century, the common understanding in the field of gunnery was that the flight path of a shell or a bullet “is nearly described by the curve of a parabola, and consequently, that the resistance of the air to the motion of these bodies is altogether inconsiderable” [3]. In 1805, Benjamin Robins stated in his paper *Resistance of the air* that a bullet always acquires a whirling motion and a progressive one and therefore he concluded that the air resistance “will be increased in that part where the whirling motion conspires with the progressive one” [3]. Hence, the deflection in motion was attributed to the difference in air resistance, and should be called the *Robins effect* since that time [4].

Gustav Magnus was a Professor of Physics at the University of Berlin during the years 1834 to 1869. His well-known experiment was conducted in 1852. It consisted of a brass cylinder held between two conical bearings to which he could impart a high speed of rotation by means of a string. He mounted the cylinder upon a freely rotatable arm and directed a current of air from a blower towards it (Fig. 1). When the cylinder was rotated, he noticed a strong lateral deviation. The spinning body always tended to deflect toward the side of the rotor that was traveling in the same direction as the wind coming from the blower. The magnitude of the deflecting forces was not measured by Magnus at that time [5]. From now on, the phenomenon was called *Magnus effect*.

In the year 1877 Lord John Rayleigh wrote an article *On the irregular flight of tennis balls* [6]. He attempted to explain the curved path of a ball in terms of the Magnus effect by calculating the Magnus force from the pressure distribution of a rotating body. At that time he also stated that it was not possible to give a complete mathematical formulation of the actual physical process since no mathematical methods were available to express the manner in which friction between the fluid and the rotating cylinder would produce circulation.

Lafay reported in 1912 about his investigations in the laboratories of physics of Ecole Polytechnique and in the Etablissement d’aviation militaire de Vincennes. He conducted experiments and demonstrated that with rotating cylinders one may attain several times the output in lift of a plane surface having the same projected area. His measurements showed how pressure and

Nomenclature

α	velocity ratio, advance ratio
α_c	critical velocity ratio
δ	flap deflection angle [deg.]
γ	location of an external vortex [deg.]
ρ	air density [kg/m ³]
ω	vector of angular velocity [rad/s]
Γ	circulation [m ² /s]
A	aspect ratio
C_L	lift coefficient
C_D	drag coefficient
C_T	torque coefficient
D	drag force [N]
\mathbf{I}	matrix of moment of inertia
\mathbf{L}	vector of angular momentum
L	lift force [N]
\mathbf{M}	torque matrix
M	pitching moment, torque [Nm]
Q	torque according to A. Thom [gr cm]

Re	Reynolds number
S_{ref}	Reference area [m ²]
St	Strouhal number
U	free stream velocity [m/s]
U_c	circumferential velocity [m/s]
a	cylinder radius [m]
c	radial distance to an external vortex [m]
c	chord length [m]
d	cylinder diameter [m]
de	endplate diameter [m]
ds	disk spacing [in]
f	frequency of vortex shedding
k_Q	torque coefficient according to A. Thom
l	cylinder length [m]
n	revolutions per second [s ⁻¹]
n_z	load factor [g]
p	roll rate [rad/s]
u	circumferential velocity [m/s]
V	free stream velocity [m/s]

suction are distributed around the cylinder and how the streamlines are deflected in the vicinity of the rotating cylinder [7]. However, a proper formula to calculate the pressure distribution around a rotating cylinder was still missing.

Hermann Föttinger wrote an article in 1918 in which he discussed experiments relating to the lateral forces acting upon

rotating cylinders placed in a current. He concluded that as far as current forces are concerned the rotor functions similarly to an inclined plate [8]. In 1919, acting upon a suggestion made by Föttinger, Professor Gumbel constructed a propeller having rotatable cylindrical blades (Fig. 2). It worked but the two scientists decided that the device had no practical value [9–11].

The most notable attempt to use the high lift forces obtainable on a spinning cylinder in an airstream was made by Anton Flettner in Germany in the 1920s. Flettner consulted with Ludwig Prandtl and the Göttingen research group (Jakob Ackeret, Albert Betz, Carl Wieselsberger et al.) on the idea of replacing the sail of a vessel with rotors. In a cross wind, the Magnus effect would

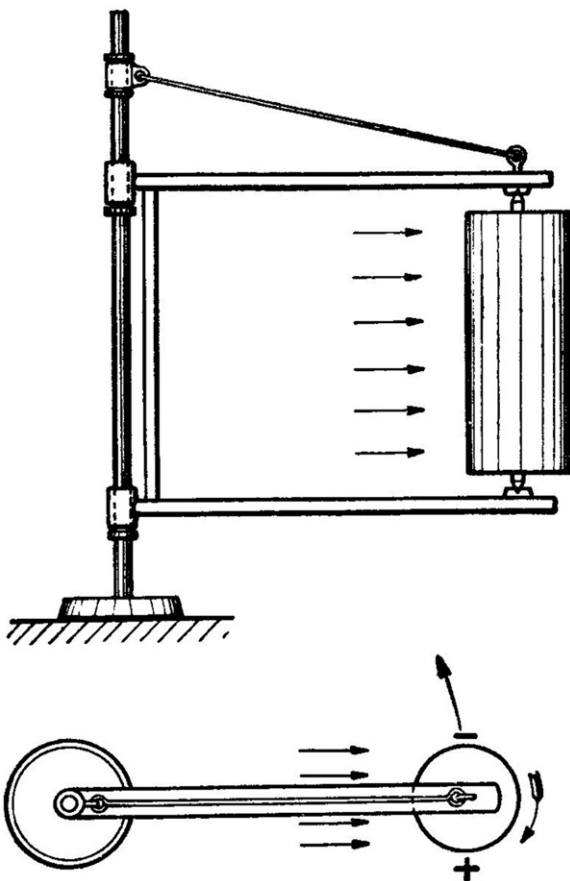


Fig. 1. Experimental setup of Gustav Magnus. Adapted from source: [24].

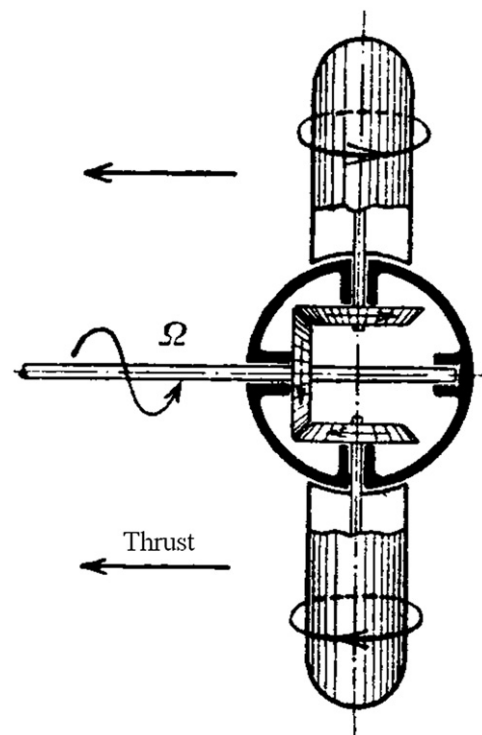


Fig. 2. Propeller with cylindrical blades according to Prof. Gumbel. Adapted from source: [9].

produce a thrust many times that for an equivalent sail area. The power to drive these rotors turned out to be a small fraction of the power required for screw propulsion. Ackeret conducted a series of wind tunnel tests on cylinders with endplates, which indicated that this method of ship propulsion was feasible. The idea of applying endplates to the rotors was suggested by Prandtl [12]. The effect of endplates doubled the lift force. Although this propulsion system was quite inexpensive for ships, the speed and reliability of screw propulsion was more than competitive. However, Flettner's inventions are still attractive for energy-optimized applications. They are still used for propulsion (e.g., Enercon E-Ship 1) or ventilation (Flettner TCX-2™ roof vent) and airplane control surfaces ('a rudder for a rudder') to this day.

The first Magnus effect investigation in the United States was made by Reid [13] at the Langley Field NACA Laboratory, using a single cylinder projecting through both sides of a five-foot diameter tunnel.

The most complete experimental work on rotating cylinders in cross-flow by then was done by Thom [14] at the University of Glasgow and reported in his doctoral thesis and in five Reports and Memoranda of the British Aircraft Research Council covering a period of nine years from 1925 to 1934 [15–19]. The effects of Reynolds number, surface condition, aspect ratio, endplates and spanwise disks were investigated by him. Thom's [16,17] publications provide a complete set of aerodynamic data for a rotating cylinder, including lift, drag, and torque coefficients.

In his review paper of 1961, Swanson provided an excellent overview on the Magnus effect and a summary of investigations [20]. His paper also includes investigations on missiles and analytical models for the Magnus effect. Besides experiments on a sole rotating cylinder, Magnus effect compound devices were tested. Calderon and Arnold [21] carried out tests on a rotating cylinder flap to evolve a high lift airfoil for STOL-type aircraft. Test flights with a test aircraft equipped with a similar rotating cylinder flap were performed and reported by Cichy [22]. Iversen [23] derived a correlation parameter for the analysis of experimental Magnus force data on the basis of the impulse or cross-flow analogy. Borg [24] prepared his report with an overview of past and future Magnus effect practical applications, which are also focused in marine applications. In Volume 1, Borg discussed the historical, theoretical, and practical aspects of the Magnus effect. In Volume 2, he described and assessed patents, which are relevant to Magnus effect devices. Borg also mentions an interesting phenomenon, the so called *Barkley Phenomenon*, which he describes as a distinct drop in drag of the Magnus rotor just prior to reaching a velocity ratio of one. This means that the resistance of the cylinder tends to disappear at that operating point. Further research is needed to characterize and quantify this phenomenon.

The most comprehensive review of work on rotating cylinders is given in the books of Zdravkovich [25,26]. These books are recommended for a profound study of the physics and application of rotating cylinders.

1.2. Magnus force

In this section, an explanation of the Magnus effect is provided. The Magnus effect is well known in sports, e.g., ball games, called 'curveball' or 'curving cross'. If a body of revolution is rotating in cross-flow, a force nearly perpendicular to its trajectory acts on the body's surface. A descriptive explanation of the Magnus effect is given by Thomson in [1]. To bear in mind in which direction the ball is deflected, Thomson explains that the spinning ball is always deflected in the direction where the 'nose' of the ball is turning to. The Magnus effect acting on a cannonball is illustrated in Fig. 3. Ball a is rotating nose down and achieves the shortest distance to the shooting position. Ball c, rotating nose up, moves



Fig. 3. Flight path of a cannonball influenced by the Magnus effect.

much farther than ball a. The nonrotating ball b is not affected by the Magnus effect, therefore its flight range is lying between ball a and ball c. The plus and minus signs indicate the reduced or increased local air pressure close to the boundary layer.

The Magnus effect is often explained by a superposition of the flow field from an ideal vortex centered in the cylinder with a uniform free stream flow. There is no viscosity in this model (no boundary layer on the cylinder) even though this is the real origin of the circulating flow. In reality, the flow around a rotating cylinder is very complex. Depending on the ratio of rotational speed, free stream speed, viscosity of the fluid, and size of the cylinder, the flow off the rear of the cylinder can separate and become unsteady. With reference to Bernoulli's potential theory, the higher velocity on one part of the body leads to a lower air pressure compared to the opposite part, where the airspeed is reduced. The potential theory is based on a frictionless flow and is a simplified explanation of the Magnus effect, which is generated due to friction within the boundary layer. Rizzo [27] discussed the fundamental principles of the Flettner rotor ship in the light of the Kutta–Joukowski theory and available experimental data. He calculated the speed of the rotor ship by applying the theory and by using wind tunnel data. His calculations showed that the results obtained from wind tunnel data are much closer to the actual speeds than those obtained by the use of the Kutta–Joukowski theory. Prandtl's [28] boundary layer theory is applicable to explain more adequately the flow around a rotating body, even the Negative Magnus Force (see Section 2.1.3). In 1929, Prandtl's theory was not generally accepted and was challenged by scientists [29].

In 1961, Swanson explained that the circulation around the rotating cylinder is a consequence of the unsymmetrical flow pattern produced by the upper and lower boundary layers separating at different positions. The circulation is then a consequence of the flow pattern as determined by the boundary layer behavior [20]. The different lengths of the laminar flow and the location of the transition or separation points within the boundary layer of the rotating cylinder are the cause for the Magnus force. Ericsson investigated a variety of body geometries, spinning in two-dimensional and three-dimensional flow, and he calls this flow phenomenon the *Moving Wall Effect*. He concluded that the Moving Wall Effect can influence the unsteady aerodynamics significantly, even in the absence of flow separation [30]. Photographs of the flow at various velocity ratios were made by Relf [31] and Prandtl [32] using a water channel. In Fig. 4, a kinetographic flow picture is given for a circular cylinder operated at a velocity ratio $\alpha = u/V = 5.5$.

Today we should better use the term *Magnus force* instead of *Magnus effect*, as the flow physics are understood by now, which lead to a force transverse to the flight path.

The Magnus force can be many times greater in magnitude than the wing lifting force, given the same projected area and dynamic air pressure. The magnitude of the Magnus force is mainly a function of the spinning rate, the flight velocity and the geometry of the body. There are secondary effects resulting from a sideslip angle and the surface roughness, which will be discussed in Section 2.

Based on a mathematical model of Bickley [33], Swanson derived equations for predicting the lift and drag coefficients of a circular cylinder of radius a by the Eqs. (1)–(3). The parameters c

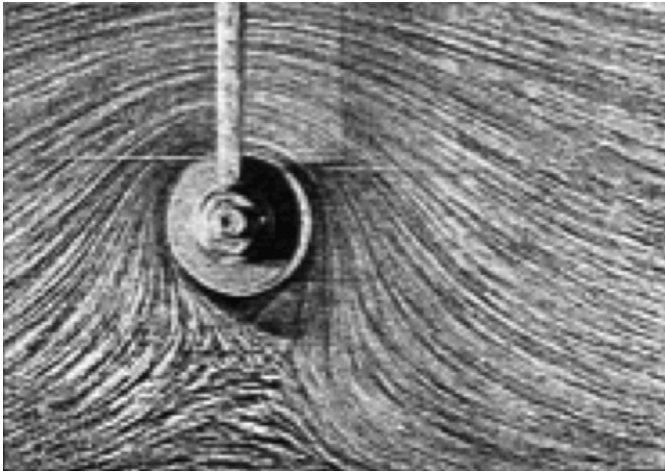


Fig. 4. Flow around a circular cylinder at a velocity ratio $\alpha=5.5$. Adapted from source: [32].

and γ are defined as the radial distance to the external vortex and the location of the external vortex, respectively.

$$C_L = \left[1 - \left(\frac{a}{c} \right)^2 \right] \cdot K_\alpha \cdot \alpha + \frac{\sin \gamma}{2\pi} \cdot \left(\frac{a}{c} \right) \cdot (K_\alpha \cdot \alpha)^2 \quad (1)$$

$$C_D = -\frac{\cos \gamma}{2\pi} \cdot \left(\frac{a}{c} \right) \cdot (K_\alpha \cdot \alpha)^2 \quad (2)$$

$$K_\alpha = \frac{1}{\alpha} \cdot \frac{\Gamma}{a \times V_\infty} \quad (3)$$

Unfortunately, there is no easy way by which the parameters a/c , γ and K_α can be determined. But these parameters have to be derived in order to get a good match for the lift and drag coefficients. An example is given for the values of $a/c=0.25$ and $\gamma=224^\circ$, where a good match is achieved for a velocity ratio range $\alpha=2-3$ [20].

In this paper, the Magnus force is considered as an aerodynamic force, which is generated if a moving surface affects the boundary layer of a lifting device. Other means such as boundary layer suction or blowing are not considered here.

There have been applications in the past using the Magnus force in two different ways, for circulation control and as a sole lifting device. Some ideas and visions of the 1920s are presented in the next section.

1.3. Ideas and visions

Flettner’s rotor ship attracted so much attention in Europe and in the USA in the 1920s that consequently many ideas and visions relating to the application of the Magnus effect were generated. In aeronautics, the rotors were designed to produce lift at minimum drag, and in maritime transport, the rotors were designed to produce thrust and for control purposes.

The following ideas can be related to three technical areas: the drive mechanism of a Magnus rotor, the combination of lifting devices, and the enhancement of the Magnus effect by various means.

1.3.1. Driving a Magnus rotor

A Magnus rotor is usable as a lifting device as long as it is spinning. In case of the rotor ship, the rotors were powered by an electrical drive system. One reason for this solution was the flexibility in selecting the spinning direction according to the wind direction and the desired moving direction. In order to

reduce system complexity and increase system safety, engineers looked for other means to drive the rotors. For example, Flettner proposed a Savonius-rotor, which is known as an auto rotating wind energy converter, to drive the Flettner-rotor. A model of a rotor ship was tested, providing such a Savonius-rotor and a Flettner-rotor mounted on top (Fig. 5).

Most of the existing rotor airplane concepts comprise a fuselage with a conventional tail and a propeller in the front. The only part which is changed, compared to a conventional airplane, is the wing. An early concept of a rotor airplane is shown in Fig. 6. This airplane model provides a molded Magnus rotor instead of a fixed wing. The purpose of using such a peculiar shape for the rotor is to provide a mechanism to rotate the wing by the air flow. The advantage of such an arrangement could be the safety in case of a motor failure, because the rotating wing continues spinning and therefore providing lift. One disadvantage would be the fixed velocity ratio between airspeed and circumferential speed, resulting from autorotation. Consequently, the lift force cannot be controlled independently from the airspeed. More details on autorotation of a Magnus rotor are presented in Section 2.1.4.

1.3.2. Combination of different lifting devices

In this section combinations of different kinds of lifting devices are discussed. The purpose of such combined devices was mainly motivated by the high lift capability of a Magnus rotor and the reliability of a wing. A rotor airplane design by Ernst Zeuzem is presented in Fig. 7, which illustrates an example of combined lifting devices. The inventor’s model provides four Flettner-rotors

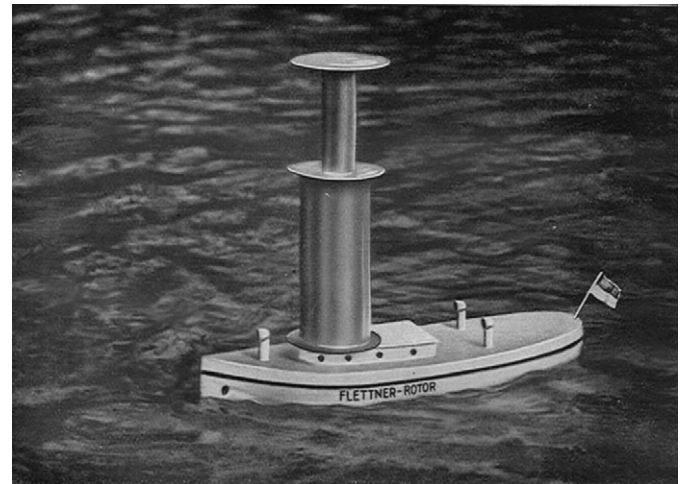


Fig. 5. Model of a sailing boat, using a Savonius-rotor to drive the Flettner-rotor mounted on top. Reproduced from source: [10], with permission of Koehler and Amelang.

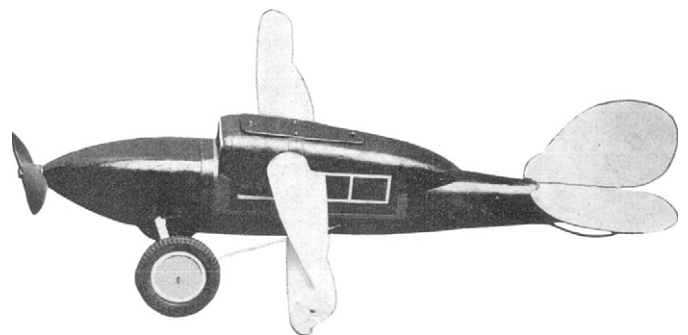


Fig. 6. Monoplano Rotor. Courtesy of Deutsches Museum Archiv.

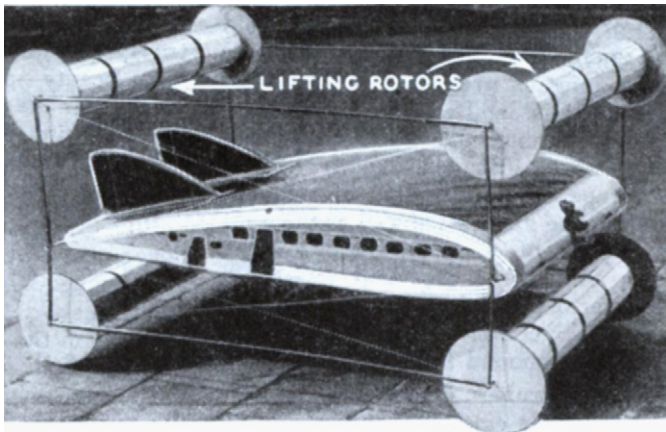


Fig. 7. Rotor airplane concept by Ernst Zeuzem, Germany. Courtesy of Deutsches Museum Archiv.

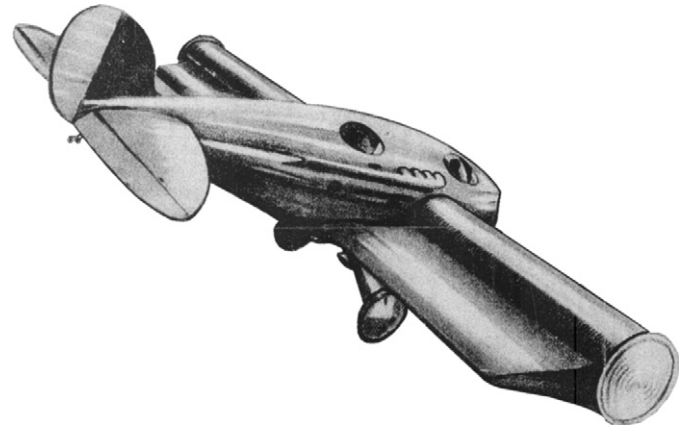


Fig. 9. Rotor airplane according to Karl Gligorin, sketch from H. and B. v. Römer. Courtesy of Deutsches Museum Archiv.

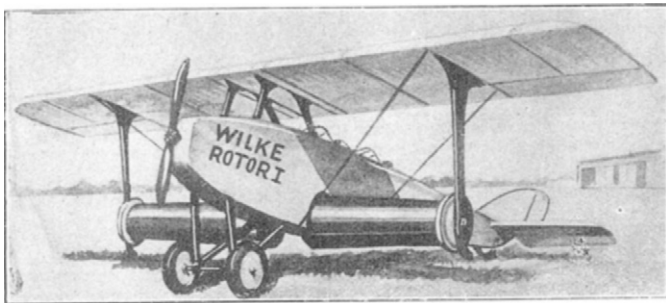


Fig. 8. Rotor airplane concept by Gerhard Wilke. Courtesy of Deutsches Museum Archiv.

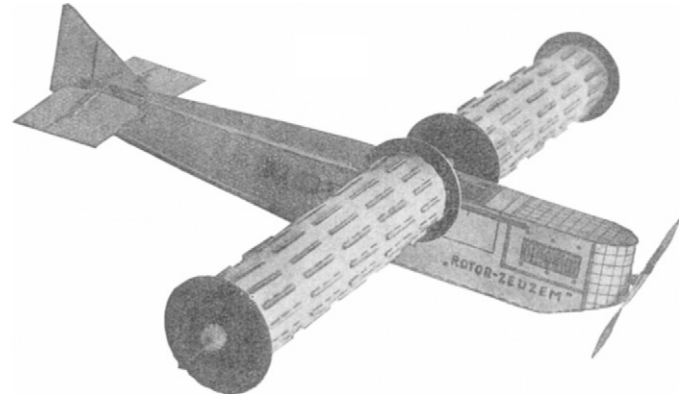


Fig. 10. Model *Rotor-Zeuzem*. Courtesy of Deutsches Museum Archiv.

which are driven by separate motors. According to the article, the passengers should be carried in the wing section designed to provide extra lift [34]. The lifting rotors underneath should work as landing gear at the same time, neglecting the fact that these rotors have to rotate the other way around to produce lift in forward flight.

A sound configuration is presented by Gerhard Wilke (Fig. 8). This concept looks like a biplane in principle. Here, the lower rotating wing should be used only as high lift device for short take off and landing. In cruise flight, the cylinder would be streamlined by movable plates to reduce drag. At low speed, the rotors should be used to enhance the lift force. Their rotational speed should be independent from the speed of the aircraft engine, which should serve as driving mechanism for the rotors [35].

A rotatable cylinder integrated at the leading edge of a conventional wing is a favorable solution for a high lift device. In 1924, Reid and Flettner [13,36] independently investigated such a compound wing for drag reduction. The Austrian Karl Gligorin designed a concept of an airplane in 1925, which comprises a compound wing (Fig. 9). The projected data of this aircraft design is taken from [37]:

- Span: 13 m
- Length: 8.6 m
- Height: 2.7 m
- Rotor diameter: 1.2 m
- Rotating speed: 550–1600 rpm
- Engine power: 550 hp
- OWE: 1050 kg
- Payload: 550 kg

- MTOW: 1600 kg
- Max cruise speed: 400 km/h

His airplane configuration comprises a conventional fuselage with one propeller in the nose, a conventional tail and control surfaces, and a compound wing with plates at the end of the rotating cylinder.

More details on compound wings are presented in Section 3.3.1 and on test aircraft in Section 3.2.3.

1.3.3. Enhancing the Magnus effect

In the beginning of the 20th century, it was understood that the rotation of the cylinder produces a circulation of the air close to the skin of the cylinder and furthermore a lift force. The idea arose that a rough surface or even bumps could improve the circulation around the cylinder and therefore enhance the Magnus effect, providing even more lift force than a smooth surface. The model of Ernst Zeuzem (Fig. 10) comprises such a rotor concept. Probably the pockmarked surface of a golf ball, called dimples, has influenced the design of the rotor. Subsequent research revealed such a surface roughness effect (more details in Section 2.1.6). Many more ideas were generated by inventors around the application of the Magnus effect, e.g., an airfoil with an integrated rotating belt. Most of them were never tested in an experiment. Some of these ideas were protected by Flettner's patents and tested in the years 1923–1928 [36,38].

More details on the aerodynamics and gyroscopic forces of a Magnus rotor are presented in the next chapter.

2. Physics of flight

A meaningful application of a rotating cylinder in aeronautics for boundary layer control or as a sole lifting device requires special knowledge about the physics of flight. On the one hand, the aerodynamics is different between a conventional wing and a rotating cylinder. On the other hand, the rotation of a cylinder implies gyroscopic forces, which affect the flight dynamics of a rotor airplane. Both topics are discussed in this chapter.

2.1. Aerodynamics of a rotating body in cross-flow

The aerodynamic coefficients of a Magnus rotor are dependent on various parameters. In this section, the characteristics of a rotating body in cross-flow and the most important parameters, such as the velocity ratio and the size of the endplates are briefly summarized. The discussion is limited to subsonic flow, although there is extensive literature available for bullets in supersonic flow which are affected by the Magnus effect as well.

2.1.1. Definition of forces and moment

As usual, the Magnus force can be divided into a lift force component perpendicular to the incoming flow and a drag force component parallel to the flow. The friction between the rotating body surface and the surrounding fluid leads to a torque, which has to be overcome by a mechanical drive. The aerodynamic coefficients C_L , C_D , and C_T are specified by the velocity ratio $\alpha = u/V$ and not by the angle of attack, as specified for wings. The aerodynamic forces are calculated as usual (4, 5). The aerodynamic moment is defined in Eq. (6) according to Thom [17]. This equation is also given in SI units for commonality (7).

$$L = C_L \cdot q \cdot S_{ref} \quad (4)$$

$$D = C_D \cdot q \cdot S_{ref} \quad (5)$$

$$M[lbf t] = C_T \cdot \rho [slugs ft^{-3}] \cdot n [s^{-1}] \cdot V [fts^{-1}] \cdot l [ft] \cdot d^3 [ft^3] \quad (6)$$

$$M[Nm] = C_T \cdot \rho [kg m^{-3}] \cdot n [s^{-1}] \cdot V [m s^{-1}] \cdot l [m] \cdot d^3 [m^3] \quad (7)$$

The reference area S_{ref} is defined as the projected surface area of the cylinder. Additional endplates or disks are not accounted for the reference area. Aerodynamic coefficients for a variety of cylinder shapes are given in Sections 2.1.6 and 2.1.10. Now, the impact of physical factors on the aerodynamics of a Magnus rotor will be explained.

2.1.2. Effect of velocity ratio

The aerodynamic characteristics of a Magnus rotor are mainly influenced by the velocity ratio between the circumferential speed of the rotor and the free stream velocity. The flow phenomenology around a circular cylinder is rather complex and consists of tip vortices and an alternate vortex shedding between the rotor ends. Thouault et al. carried out a numerical flow visualization around a rotating cylinder at $Re=72,000$ [39]. The results are presented in Fig. 11, which shows a variety of 2D flow patterns in terms of the velocity ratio α . The first ratio presented ($\alpha=0$), corresponds to a non-rotating cylinder in free stream. The other flow patterns show gradual changes with rising α as follows:

The Kármán vortex street is seen for $\alpha=0-2$. The eddies are formed and shed alternately on two sides of the cylinder. The long eddy formation at $\alpha=0$ is considerably shortened for higher α . Vortex formation and shedding can no longer be seen for $\alpha > 2$. The near wake is reduced in length and width and biased towards the side where u and V are in opposite directions.






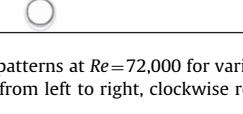
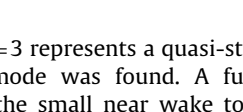
$\alpha = 0.0$ $St = 0.20$		First shedding mode. Alternate vortex shedding of Von Kármán type
$\alpha = 1.0$ $St = 0.26$		
$\alpha = 2.0$ $St = 0.46$		
$\alpha = 3.0$		Quasi-steady flow. Closed streamlines around cylinder. Two stationary vortices located on the cylinder lower side.
$\alpha = 3.5$ $St = 0.02$		Second shedding mode. Only one vortex is shed
$\alpha = 4.0$		Quasi steady flow. Flow topology is comparable to the potential theory solution
$\alpha = 6.0$		

Fig. 11. Flow patterns at $Re=72,000$ for various Strouhal numbers St and velocity ratios α (flow from left to right, clockwise rotation) [39].

The case $\alpha=3$ represents a quasi-steady-state. At $\alpha=3.5$ a second shedding mode was found. A further increase in α towards 4 deflects the small near wake to the side where u and V are in opposite directions. The case $\alpha=6$ represents a single large eddy.

Mittal and Kumar [40] investigated the two dimensional flow past a rotating cylinder at a very low Reynolds number $Re=200$. One of the objectives was to determine the effect of rotation of the cylinder on vortex shedding. They found that the cylinder resumes vortex shedding at $\alpha=4.4$ and continues till $\alpha=4.8$. Fig. 12 shows the phase diagrams of C_L and C_D for the fully developed solution. The unsteadiness in the aerodynamic coefficients is caused by vortex shedding.

It is known that vortex shedding occurs for Reynolds numbers all the way up to at least $Re=8 \times 10^6$ [25]. Therefore, the control of vortex shedding is of significant practical interest in many engineering applications and could be realized for example by controlling the angular velocity of the rotating body. For all Reynolds numbers for which vortex shedding from a rotating cylinder occurs, there is always a critical velocity ratio α_c beyond which shedding ceases. In general, increasing the Reynolds number causes the second shedding mode to appear earlier and last longer with respect to α .

The Strouhal numbers (St), given in Fig. 11 and defined in Eq. (8), describe the oscillating flow past a rotating cylinder.

$$St = \frac{f \cdot d}{V} \quad (8)$$

A low Strouhal number ($St \leq 10^{-4}$) indicates a quasi-steady flow. Fig. 13 shows the results of an experimental investigation of the vortex shedding characteristics of a low aspect ratio rotating cylinder ($A=5.1$) at $Re=4 \times 10^4$, obtained by Badalamenti and Prince [41], Diaz [42], and Tanaka [43]. The critical velocity ratio was found to be $\alpha_c=2$ and the Strouhal number St increased with increasing velocity ratio.

For this case ($\alpha=2$) the flow phenomenology is presented in Fig. 14. The flow separates on each front edge of the endplates and

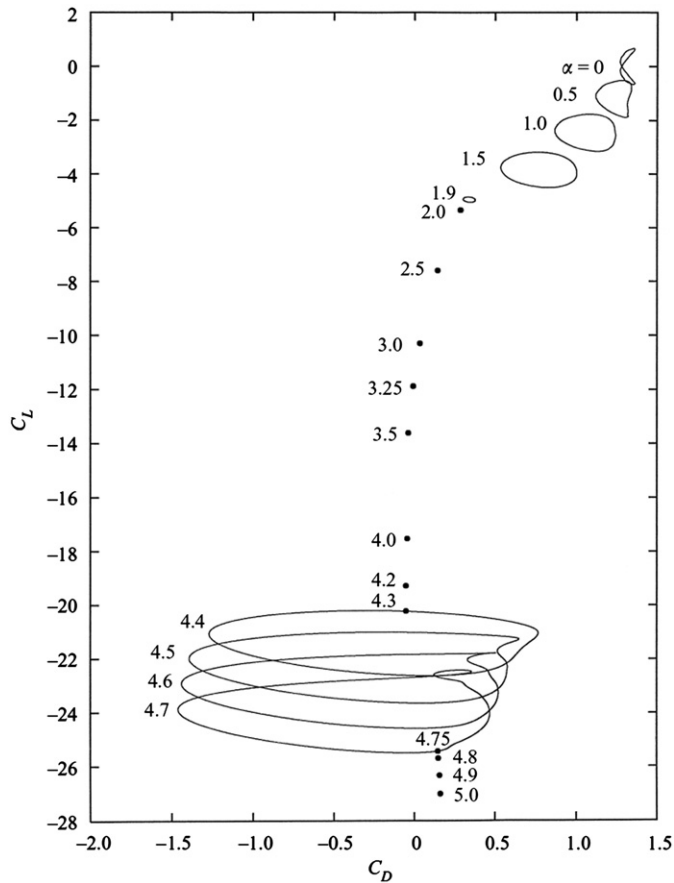


Fig. 12. Phase diagrams of C_L and C_D for various values of α . © 2003 Cambridge University Press, reprinted from [40] with permission.

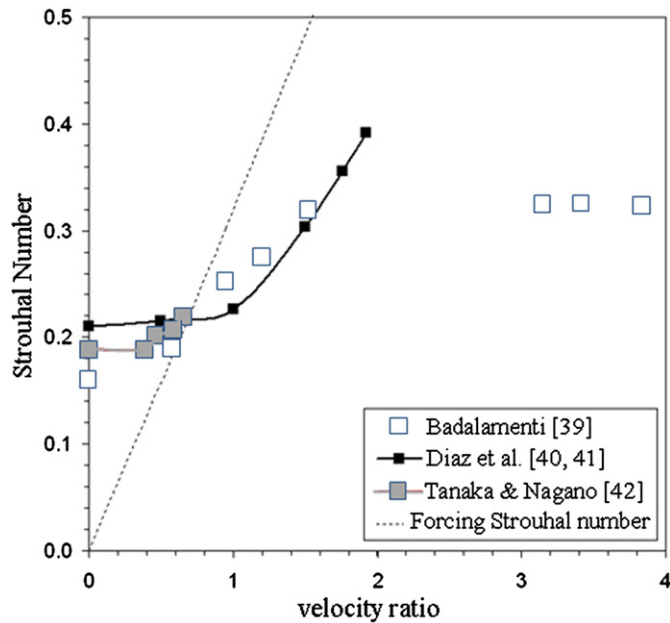


Fig. 13. Strouhal number St variation with velocity ratio α , reprinted with permission by the author [41].

on the rear of the cylinder. The tip vortices merge further downstream. Between the endplates the shedding of Kármán type is observed.

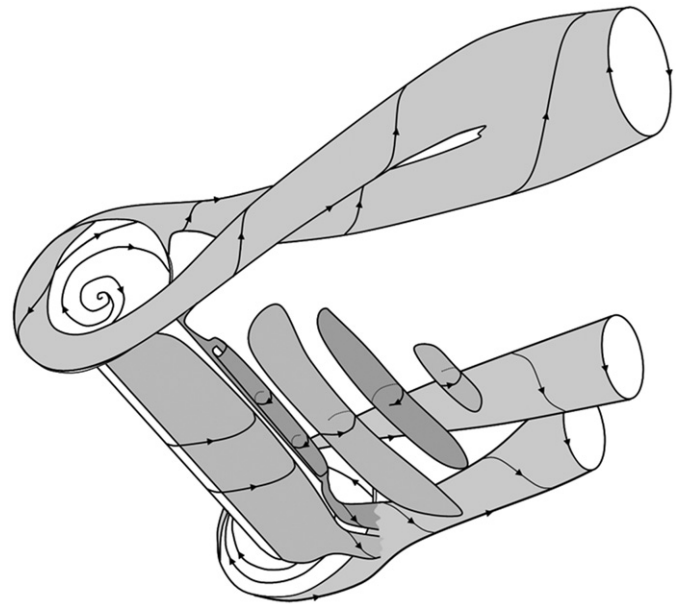


Fig. 14. Flow phenomenology of a cylinder with endplates rotating at $\alpha=2$ in cross-flow from left [39].

2.1.3. Negative Magnus force

Lafay [7,44] was one of the first researchers to find a side force in the opposite direction to that predicted by Magnus [5]. This phenomena was investigated amongst others by Ericsson [30,45,46] and Fletcher [47]. Swanson gave a thorough review of the phenomena [20]. This negative Magnus force can be observed in a certain range of the Reynolds number and at low velocity ratios. The origin of the negative Magnus force was attributed to different locations of the transition points on both sides of the rotating cylinder, where the laminar flow either turns to turbulent flow or separates [48]. The maximum value of the negative lift force coefficient $C_{L,min} = -0.6$ was found at approximately $Re = 3 \times 10^5$ for a velocity ratio $\alpha = 0.2$. Below $Re = 99k$ and above $Re = 501k$ the inversion of the Magnus force disappears. Thom [17] found that this phenomenon is also dependent on the surface roughness of the cylinder. Whereas a plain brass cylinder showed a negative lift coefficient, a cylinder with sanded surface showed a positive lift coefficient under the same condition.

The negative Magnus force is an issue for the design of a rotor airplane, because in the Reynolds number and velocity ratio range mentioned above the lift force could break down without any indication. This topic will be discussed in more detail in Section 4.2.

2.1.4. Autorotation

It has already been mentioned that rotation is necessary to produce lift by a Magnus rotor. Besides using a mechanical drive it is possible to use autorotation, if the rotor is capable to do so. A circular cylinder is not capable of autorotation. This is a disadvantage as in the case of a motor failure the lift drops with the rotary speed of the cylinder. But there are other kinds of Magnus rotors which are capable of autorotation. Lugt [49] provided a general overview of the literature on autorotation. The body of an auto rotating device is geometrically shaped in such a way that, whenever it is kept fixed in a fluid flow, a torque is created that initiates rotation as soon as the body is released. A flat plate and a thin elliptic cylinder are typical bodies capable of autorotation. Other shapes like cruciform plate arrangements, triangles, and squares can autorotate as well. The cup-anemometer and the

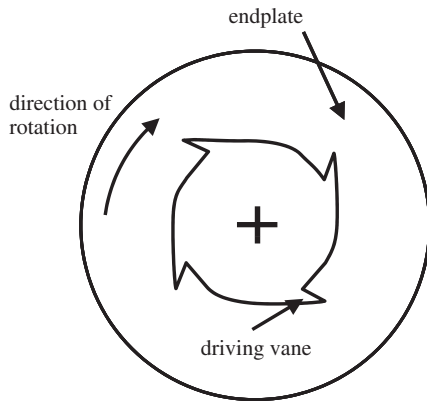


Fig. 15. Four-vaned cylindrical Magnus rotor, according to [51].

Savonius rotor are well known examples of an autorotor. The Savonius rotor appears to have the highest rate of autorotation $\alpha=1.37$ among the Magnus rotors investigated by Iversen [50]. Miller [51] performed wind tunnel experiments for an irregular shaped cylindrical Magnus rotor, see Fig. 15. The steady state velocity ratio during the tests was $\alpha=0.46$. The resultant lift and drag coefficients computed by integrating the measured pressure distribution data revealed the cyclic nature of the lift and drag with time. Lift coefficients for several Magnus rotors including a rotating cylinder and a thin elliptic cylinder were presented by Zaic [52]. The conclusion is that an autorotation capable Magnus rotor could be used as an alternative to a non-capable one with a mechanical drive. But the achievable velocity ratios are low and therefore the maximum lift force is low, too.

As this article reviews the Magnus effect in aeronautics, another interesting finding should be noted in connection with autorotation. Salter [53] refers to an article of Skews [54], who examined the autorotation of prisms whose cross-sections are regular polygons. Salter draws attention to a new method for aircraft accident investigation. The free glide angles for autorotating broken pieces of aircraft are specified as an angle of 45° for objects like a wing. By measuring the spread of debris, the height of the break-up can be estimated.

2.1.5. Effect of Reynolds number

It has previously been established that the magnitude of lift and drag of a rotating cylinder at low velocity ratios $\alpha < 1$ shows a significant dependency on Reynolds number in terms of lift variation [20,55]. For Magnus rotors, the Reynolds number is based on the cylinder diameter. The effect is particularly pronounced when $Re > 6 \times 10^4$. In addition, the results also seemed to suggest that a second region of Reynolds number dependency may exist for a velocity ratio $\alpha > 2.5$ and $Re < 4 \times 10^4$ [55]. Under these conditions all the curves indicated the same trend, but a slight increase in lift was noted as Re decreased. A similar effect was seen in the drag data. The earlier work by Thom [16] in 1925 appears to support this trend in drag variation. However, both authors state a little lack of confidence in the accuracy of the results at the Reynolds numbers and velocity ratios in question.

2.1.6. Effect of surface roughness

In general, surface roughness affects the boundary layer flow. Advantages and disadvantages of applying a rough surface to a Magnus rotor are briefly summarized in this section.

The surface of a golf ball is typically not smooth. The effect of the dimples of a golf ball is to delay separation of the boundary

layer by inducing transition to turbulent flow. The result is a drop in drag from about $C_D=0.4$ to 0.1 [56].

Pressure drag is connected to flow separation, where earlier separation in general leads to higher pressure drag. With the help of a simple test setup, Thomson [1] explained the effect of surface roughness of balls. He demonstrated that the pressure difference measured on a rotating rough ball in a flow is more than twice that for the smooth ball.

Luo et al. [57] studied the effect of surface roughness on the side force acting on an inclined ogive cylinder. The cylinder was coated with aluminum oxide particles with a relative roughness of $d_{\text{particle}}/d_{\text{cylinder}}=0.0093$. Their results showed that this surface roughness is capable of triggering the laminar to turbulent transition in the boundary layers of the ogive cylinder at a Reynolds number of 3.5×10^4 . At certain roll angles the boundary layer on both sides of the cylinder appeared to be turbulent, but at other roll angles, only one of the boundary layers was turbulent.

Thom [17,18] also examined the effect of surface roughness on the lift and drag forces for the Reynolds number range $33k < Re < 93k$. He glued sand onto the cylinder surface but did not specify the relative roughness. The lift and drag coefficients are slightly increased for the sanded cylinder compared to the plain cylinder. In Fig. 16 the comparison of the lift coefficients of a smooth, a wooden, and a sanded cylinder is presented.

Furthermore, Thom measured the torque of a rotating cylinder in still air and for Reynolds numbers between $33k < Re < 93k$ [17]. He derived torque coefficients out of his results by introducing his own formulas. His formulas have to be applied carefully, as he utilized unusual units compared to today's standard units (see Eq. (6)).

One of his findings was that at low air speed rotation has the effect of reducing the air torque below that in still air, and that thereafter the torque increases with increasing air speed.

Besides studies on the surface roughness of a lone rotating cylinder, extensive studies on airfoils with an integrated rotating cylinder were performed in the last decades. Modi et al. [58] made a comprehensive study involving wind-tunnel investigation, numerical simulation, and flow visualization which demonstrated that the momentum injection through Moving Surface Boundary Layer Control (MSBC) results in a significant delay in the stall angle (up to 50°) and an increase in the lift coefficient. The airfoil performance can be improved further by

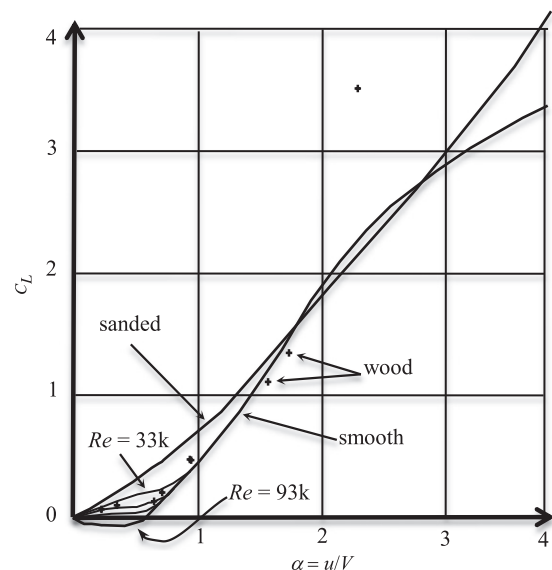


Fig. 16. Surface roughness effect on the lift coefficient. Data according to Thom [17].

proper selection of the cylinder surface condition. The cylinder with axial splines was found to be the most effective. Fig. 17 shows the effect of surface roughness and momentum injection on the lift coefficient of an airfoil, where a rotating cylinder is integrated in the leading edge.

For the smooth cylinder case, as expected, the lift coefficient first dips at stall, but is then followed by a monotonic rise with an increase in the angle of attack in the range tested ($\text{AoA} < 50^\circ$), in the absence of a momentum injection.

Moreover, a reduction in the drag coefficient was found. For example, the drag coefficient for $\text{AoA}=30^\circ$ was reduced from $C_D=1.6$ for the smooth cylinder case without momentum injection ($\alpha=0$) to $C_D=0.7$ for the airfoil with a splined cylinder at $\alpha=2$ [58]. The conclusion is that the performance of an airfoil with an integrated cylinder is enhanced, as the lift coefficient increases and the drag coefficient decreases, in particular if the surface of the cylinder is splined [58].

The effect of surface roughness on the lift and drag coefficients of a lone rotating cylinder is very small, but the air torque is approximately doubled for the sanded surface. Fig. 18 shows the resulting torque coefficient for three cylinders with different surface roughness. It clearly indicates the higher torque for a rough surface

2.1.7. Effect of aspect ratio

The effect of wing aspect ratio of wings is similar to rotors. Swanson concluded in his review paper that a general trend is indicated by experimental data due to the aspect ratio of rotors: The smaller the aspect ratio the smaller the maximum lift

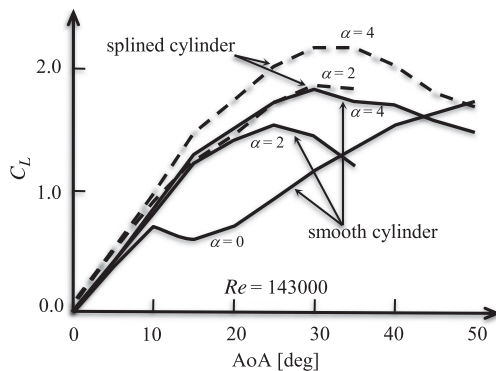


Fig. 17. Comparative study showing the effect of surface roughness and momentum injection on the lift coefficient at high angles of attack and varying velocity ratio α . Data according to [58].

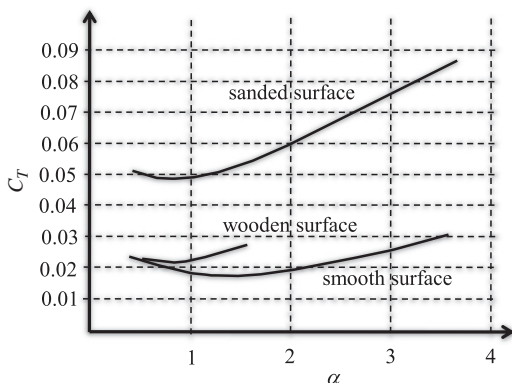


Fig. 18. Torque coefficient for a cylinder rotating in an air stream, data according to [17].

obtained and the smaller the velocity ratio at which this maximum is reached [20]. Leakage flow and consequent pressure equalization around the ends of the cylinder is responsible for this aspect ratio effect. For wind tunnel testing, a good approximation to two-dimensional flow is obtained by extending the cylinder through the tunnel walls with a very small clearance. The only investigation using such an apparatus seems to have been made by Reid [13]. Other attempts have been made to approach two-dimensional or infinite cylinder end conditions. The closest approach to infinite cylinder conditions is believed to have been obtained with a three-section apparatus used by Swanson [59]. One of the primary objectives of this investigation was to determine whether or not a maximum lift coefficient of $C_L=4\pi$ could be obtained as predicted by Prandtl [60] at a velocity ratio $\alpha=4$, when both stagnation points would coincide at the bottom of the cylinder. His prediction was based on his well-known kinetographic flow pictures, which show the streamlines around a rotating cylinder at a very low Reynolds number [32]. Contrary to Prandtl's prediction, Swanson demonstrated that the Magnus lifting force was still increasing up to a velocity ratio of 17 providing a lift coefficient of $C_L=14.3$, which is more than 4π .

It can be concluded that higher lift forces can be achieved if the aspect ratio of a Magnus rotor is increased.

2.1.8. Effect of rounded ends

Another important parameter influencing the flow around a rotating cylinder and therefore the aerodynamic coefficients is the shape of the cylinder ends. Thom [16] examined the effect of square and rounded ends on the flow around the rotating cylinders with a length $l=350$ mm and a diameter $d=80$ mm. In Figs. 19 and 20 it is depicted that the lift and drag slope decreases likewise for a cylinder with rounded ends above a velocity ratio of around 2. It is interesting to mention that a rotating sphere provides more drag than lift for the investigated velocity ratios.

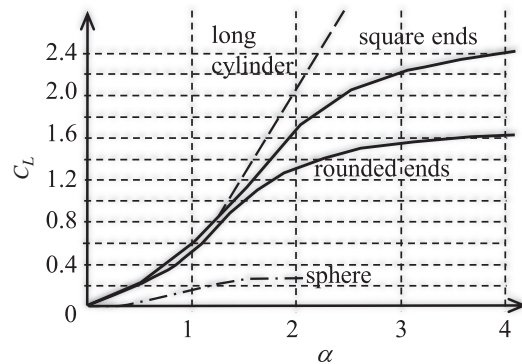


Fig. 19. Effect of rounded ends on lift coefficient, data according to [16].

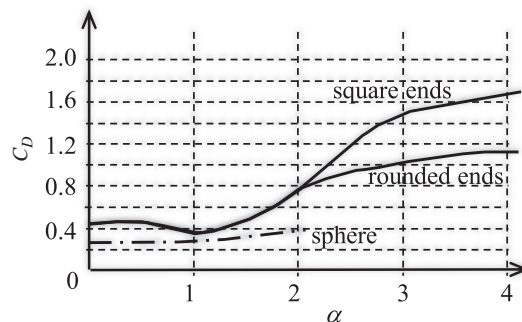


Fig. 20. Effect of rounded ends on drag coefficient, data according to [16].

2.1.9. Effect of disks

The first prominent Magnus effect application, the Flettner rotor, was mounted with endplates. The idea of applying endplates to the rotors was suggested by Prandtl in 1924 [61]. Ten years later, Thom [18] investigated the effect of large endplates up to an endplate-to-cylinder diameter ratio $de/d=3$. The existing studies suggest that the addition of such an endplate causes the lift coefficient, produced at high velocity ratios ($\alpha > 2$), to be approximately doubled. Busemann [62] investigated the effect of endplates with a short cylinder of aspect ratio $A=1.7$ and with a long cylinder of $A=12$. He added endplates with a diameter ratio between $1.5 \leq de/d \leq 3$. Busemann concluded that above a velocity ratio of $\alpha=4$ the nearly linear increase in lift can be further increased by enlarging the endplate size. The lift increasing effect turned out to be negligible for small velocity ratios ($\alpha < 2$).

Recent research was done by Badalamenti [55] for a cylinder with aspect ratio $A=5.1$ and diameter ratios ranging from $de/d=1.1$ to 3. The results clearly show the effect of endplate size on lift and drag in Figs. 21 and 22. Increasing the diameter ratio de/d has a similar effect as an increase in aspect ratio mentioned above, increasing the maximum attainable lift, and delaying the occurrence of this maximum to higher velocity ratios. The relationship between plate size and the increase in the maximum lift coefficient is rather proportional. One could say that, for a given plate size, the ratio of the maximum lift coefficient relative to that for the no endplate case was approximately equal to the ratio de/d . Thouault et al. [39] verified the experimental data of Badalamenti using Unsteady Reynolds Averaged Navier-Stokes (URANS) simulations.

The nature of the lift and drag curves result in the peak lift-to-drag ratio occurring at fairly low α . Fig. 23 shows that the peak was generally close to $\alpha=2$, but that its exact position was nearly independent on endplate size. The magnitude of C_L/C_D was substantially increased beyond that with no endplates only when $de/d > 2$.

The ability of larger endplates to reduce the induced drag component is shown in Fig. 24. The reason is said to be an effect similar to increasing the aspect ratio.

The choice of endplate size for the best drag performance was found to be dependent on velocity ratio. At low velocity ratios ($\alpha < 1$), smaller plates generally gave slightly smaller drag. For

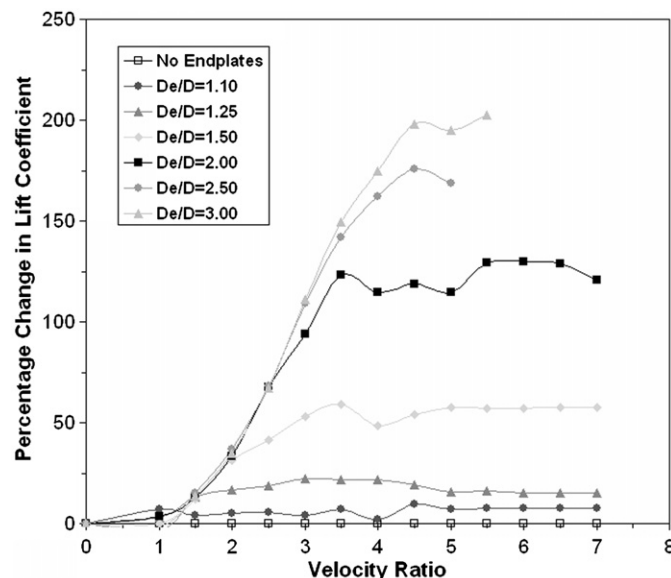


Fig. 21. Effect of endplates on lift coefficient [55], reprinted with permission from AIAA.

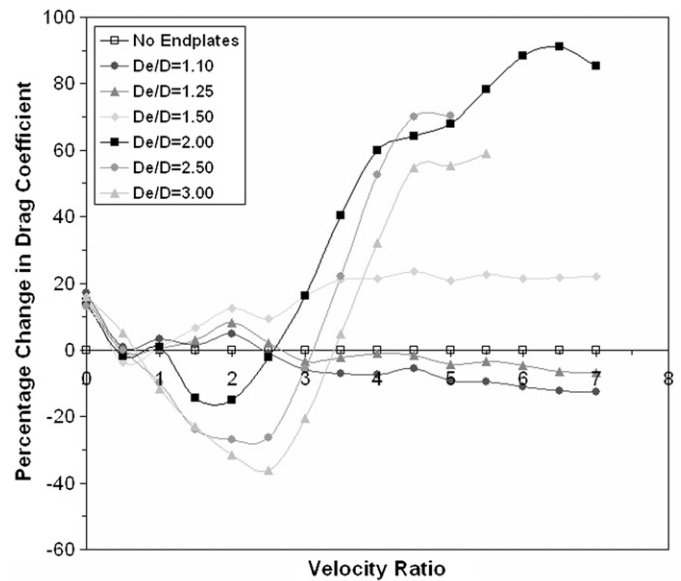


Fig. 22. Effect of endplates on drag coefficient [55], reprinted with permission from AIAA.

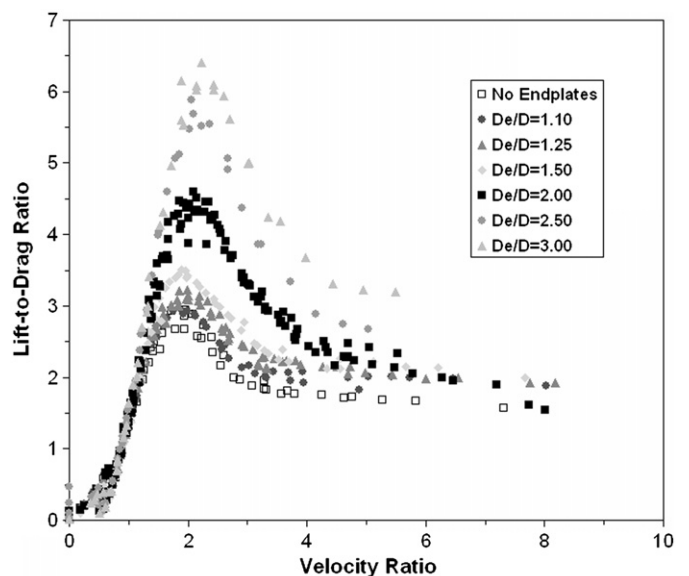


Fig. 23. Lift over Drag [55], reprinted with permission from AIAA.

applications at moderate velocity ratios ($1 \leq \alpha \leq 3$), larger plates are preferred, so as to delay the increase in induced drag. For high velocity ratio applications ($\alpha > 3$), smaller plates are again more desirable as the drag quickly approaches a limit [55].

Thom [18] was the first to investigate the effect of spanwise disks. He added equally spaced disks along the span of a rotating cylinder with a relative distance of $0.75d$ and $1.25d$. Fig. 25 shows a significant rise in C_L for velocity ratios above 5. The negative drag in the range of $4 < \alpha < 7$ is particularly unexpected, which indicates that the inclination of the resultant force is tilted upstream. With respect to the phase diagrams of Mittal, presented in Fig. 12, it is assumed that Thom measured most likely the negative peaks of the indicated values, not being aware of the oscillations occurring in this velocity ratio range.

The significant rise in C_L may be attributed to the flow around 17 disks mounted on the rotating cylinder investigated by Thom.

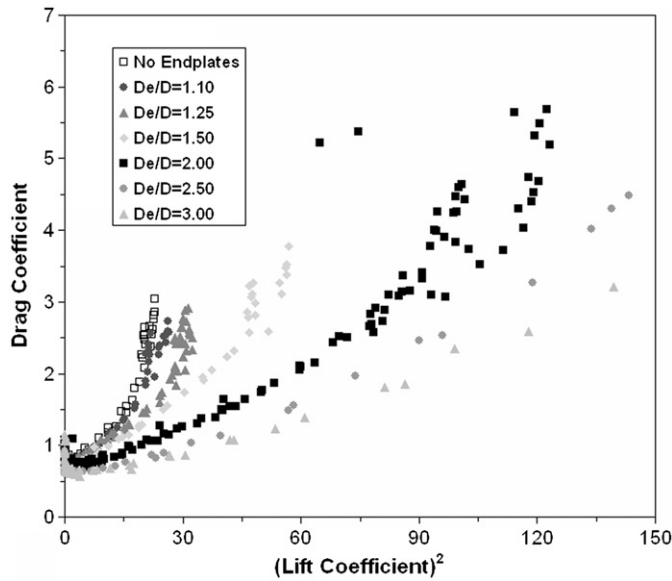


Fig. 24. Effect of endplate size on induced drag [55], reprinted with permission from AIAA.

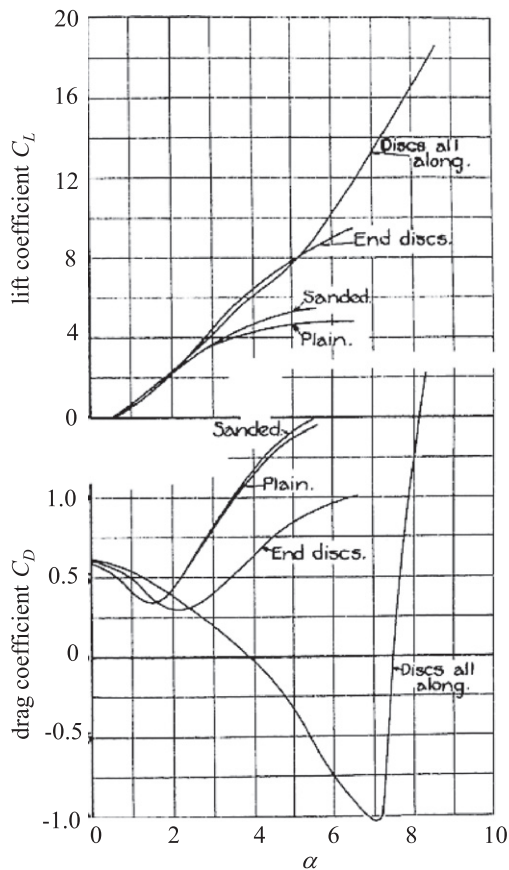


Fig. 25. Lift and drag coefficients of a Thom-rotor [18].

The total lift is produced by the combined action of the rotating cylinder and its disks.

Thouault et al. [63] recently investigated the effect of spanwise disks using URANS simulations. The results are limited to a velocity ratio $\alpha \leq 3.4$, but they provide insight into the manipulated boundary layer. First of all, the streamwise velocity component increases between the boundary layers of two facing disks

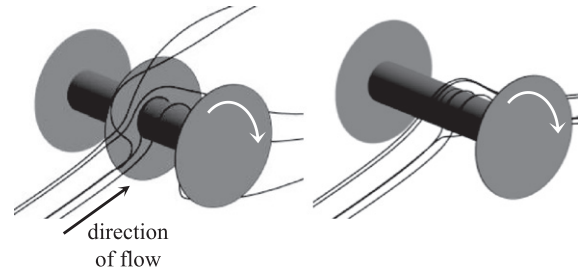


Fig. 26. The radial flow component effects the boundary layer close to the disks [39].

thereby decreasing the effective velocity ratio. Secondly, at the corner between cylinder and disk, the cylinder boundary layer thickness is reduced due to the radial flow component occurring on the disk. The significant radial flow component on the disk is evidenced by flow visualization near the middle disk in Fig. 26. The incoming flow located near the disk is entrained by the disk boundary layer in the radial direction. In addition, a velocity component in the spanwise direction (toward the disk) is observed. Further, adding spanwise disks decreases the strength of the tip vortices. The combination of these three effects leads to a drag reduction at high α compared to a cylinder configuration without spanwise disks.

Thom calculated the power to drive a cylinder with spanwise disks. Unfortunately, he mistakenly concluded that, “the enormous power which is apparently necessary to give the very high rotational speeds makes the idea impracticable”; cited from [18]. Thom skipped further investigations due to this erroneous calculation. This mistake was identified 60 years later by Norwood [64]. He discovered that Thom made a scaling error by using a torque coefficient for a wrong Reynolds number. Instead of 4830 hp, which was the result of Thom’s calculation, Norwood found the correct value of 118 hp.

2.1.10. Summary of aerodynamic coefficients

This section briefly summarizes the experimental data on rotating cylinders available in the literature. The diagrams shall provide a quick overview on the maximum values and trends of the aerodynamic coefficients for lift, drag and torque. A comparison between different cylinder geometries and surface roughness is provided.

Fig. 27 shows the lift and drag coefficients of the so called Flettner-rotor, a rotating cylinder with endplates. The experiments were conducted by Ackeret et al. [60,65,66] to investigate the effect of endplates and the data was used to design the first rotor ship *Buckau*.

Fig. 28 shows a collection of torque coefficients C_T for different Magnus rotors, plotted over rotational speed. The dependency on Reynolds number and surface roughness is demonstrated. The highest torque coefficient is found for cylinders with spanwise disks, which is about 30 times higher compared to a plain cylinder. The torque coefficient C_T shall be used with Eq. (7) given in Section 2.1.1. to calculate the aerodynamic torque.

The aerodynamic efficiency is usually given as the ratio between lift and drag. For a variety of Magnus rotor types the aerodynamic efficiency is plotted in Fig. 29. The maximum value of C_L and of C_L/C_D is additionally marked for each rotor type. A Thom-rotor with spanwise disks produces the highest aerodynamic efficiency compared to other Magnus rotors. The maximum value of 40 is given for a velocity ratio of $\alpha = 5.7$.

In relation to a double slotted Fowler flap, which provides a maximum lift coefficient of $C_{L,max} = 3.5$ at an efficiency of $C_L/C_D = 15$ [67], the Thom-rotor performance is impressive.

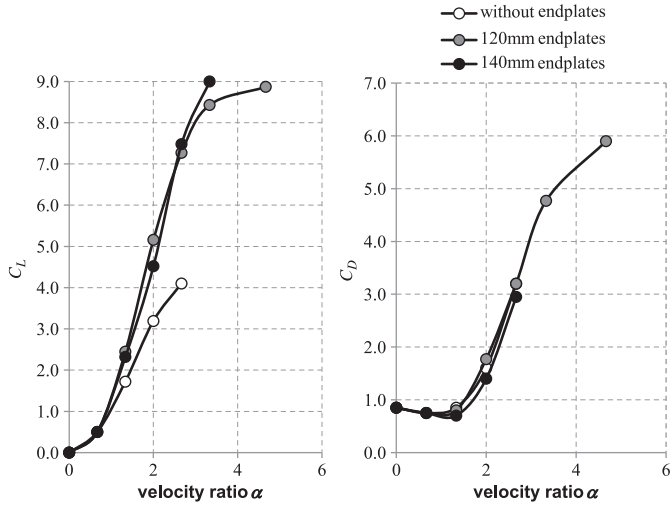


Fig. 27. Lift and drag coefficients of a Flettner-rotor, data according to Ackeret [65].

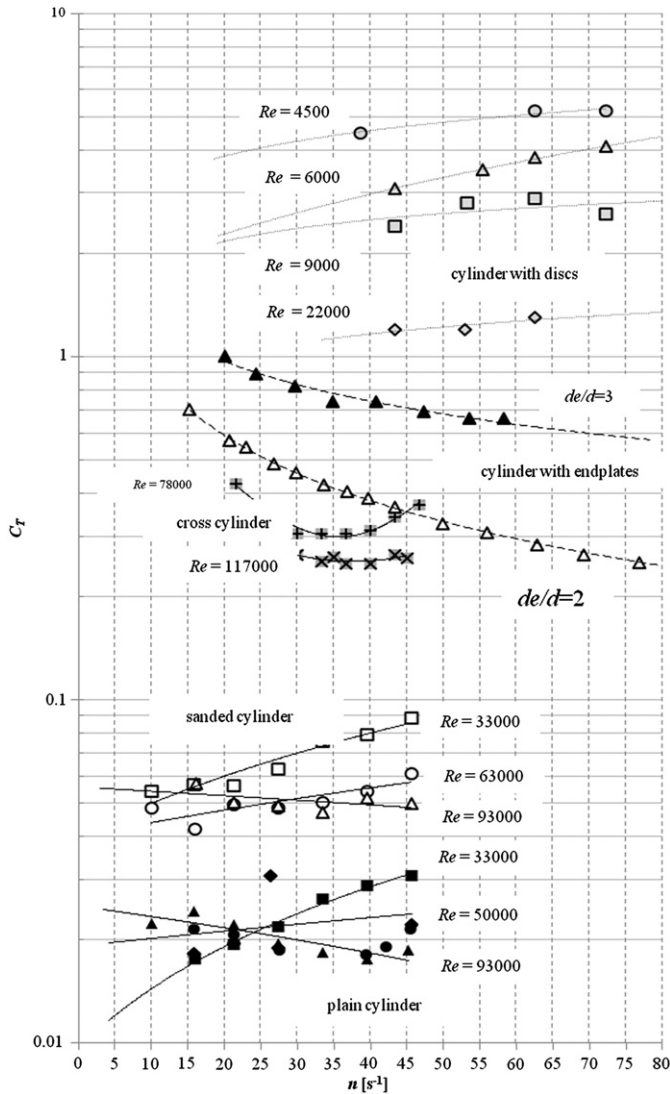


Fig. 28. Torque coefficient C_T for different circular cylinders, data according to Reid [13], Thom [17,18], Badalamenti [55].

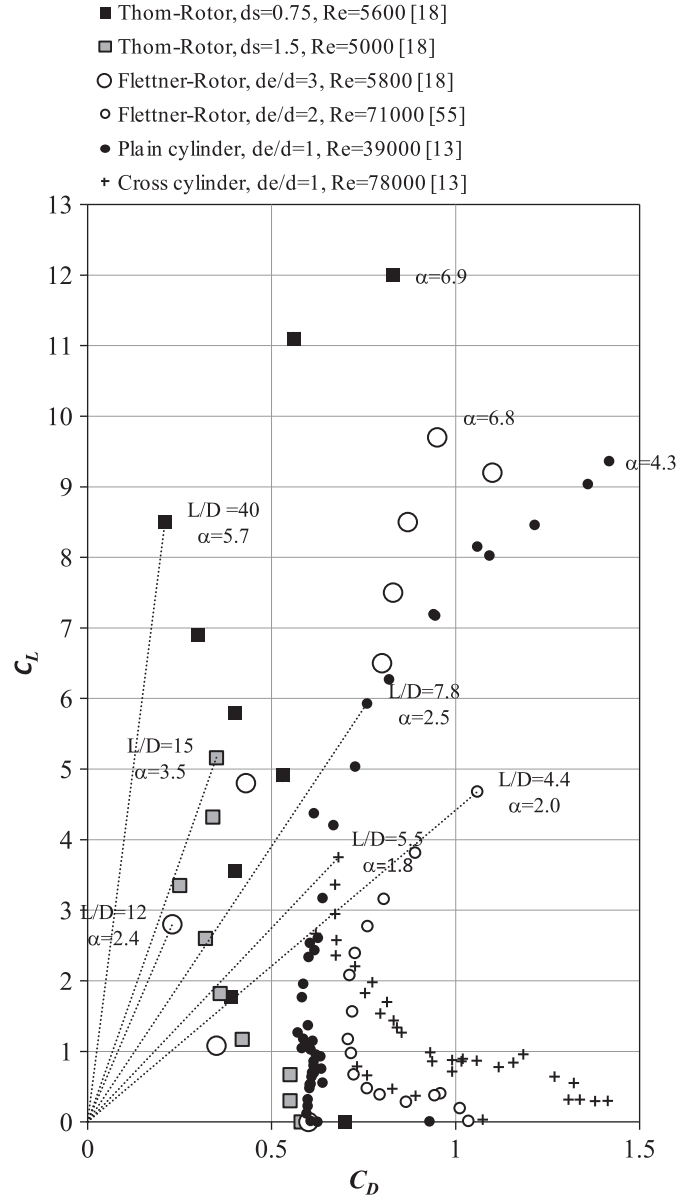


Fig. 29. Aerodynamic efficiency of Magnus rotors, data according to [13,18,55].

However, the power consumption to drive the Thom-rotor is high. The maximum efficiency of a conventional helicopter rotor is around $C_L/C_D=7$ [68]. This value can be achieved by a Flettner-rotor as well.

Rotors with spanwise disks (Thom-rotor) are a good choice if the rotor-length is limited by the rotor airplane requirements. However, more power is required to drive the Thom-rotor. In most cases, the Flettner-rotor is the best trade-off between power consumption and aerodynamic efficiency, and is therefore recommended for applications in aeronautics. Fig. 30 shows the effectiveness of three Flettner-rotors with different endplate sizes.

2.2. Gyroscopic forces on a Magnus rotor

A Magnus rotor is typically spinning at high rates, particularly at low airspeed to produce enough lift for take off and landing. There are two gyroscopic effects which influence the lateral motion of an aircraft and therefore are one of the major issues to solve for a controlled flight: the precession and the nutation.

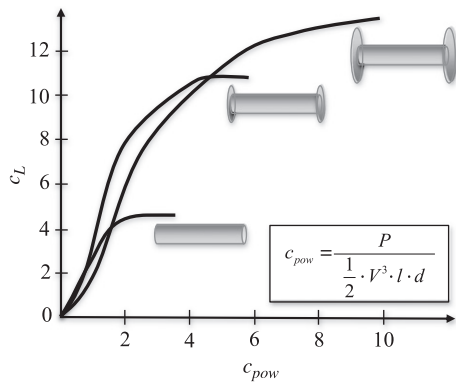


Fig. 30. Effectiveness of Flettner-rotors with different endplates sizes, data according to [55].

The torque-induced precession is a change in the orientation of the rotation axis of a rotating body. It is based on a gyroscopic force which can be explained using the principle of conservation of angular momentum. A spinning cylinder tends to resist changes to its orientation due to its angular momentum. In physics, this effect is also known as *gyroscopic inertia*.

The behavior of a gyroscope is explained on the basis of the main law of rigid body dynamics according to which the time rate $\partial \mathbf{L} / \partial t$ of change in the angular momentum \mathbf{L} equals the torque \mathbf{M} of the external forces exerted on the body:

$$\frac{\partial \mathbf{L}}{\partial t} = \mathbf{M} \quad (9)$$

The review of Potts et al. [69] on air-vehicles with circular planform (disk-wings) provides an analysis of the effect of gyroscopic forces on the flight dynamics of a spinning lifting device. Such Frisbee-like air-vehicles are typically unstable in the pitch axis and must be inertially stabilized by spinning. If the disk is rotating, gyroscopic effects dictate that this pitching moment results in a rolling rate. For a disk rotating in the direction of positive yaw, a positive pitching moment will generate a negative roll rate.

$$p = -\frac{M}{I_{zz}\omega_z} \quad (10)$$

The induced roll rate, as given in formula (10) is proportional to the magnitude of the aerodynamic pitching moment M , but it is inversely proportional to the angular momentum of the rotating disk $I_{zz} \times \omega_z$. This knowledge on precession translated to the flight dynamics of an air vehicle with rotating cylinders leads, for example, to a yawing motion, if a rolling moment was induced. At fast rotation this precession occurs very slowly. An interesting VTOL air vehicle concept was proposed by Gress [70], which uses gyroscopic forces of tilting lift fans for flight control.

Nutation is a slightly irregular motion of the rotation axis. It can be observed if a gyroscope shows precession and, in addition, is disturbed by an external force. The effect of nutation might be observed as tumbling, as yaw and roll angles are expected to oscillate at the same time.

3. Applications

The Magnus effect has been a well known phenomenon at least since the mid 19th century, but did not lead to any commercial application until the year 1924 when the first rotor ship, using Flettner-rotors, was invented and presented in Germany. This was the beginning of a short period when inventors and engineers pushed the technology of rotating cylinders. Nineteen patent applications of Magnus effect devices for

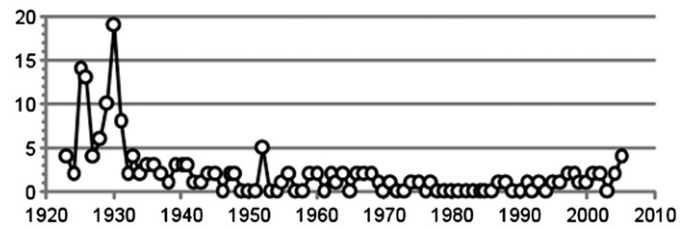


Fig. 31. Number of patent applications worldwide per year for applications of the Magnus effect in aeronautics.

aeronautical purposes¹ in 1930 indicate the impact of Flettner's rotor ship on industry (Fig. 31).

None of Flettner's two rotor ships, named *Buckau* and *Barbara*, were commercial successes. The Flettner-rotor worked fail-safe but the era of sailing ships and steam engines was over. In times of high oil prices, the need for alternate sources of energy, such as wind energy, brings Flettner's idea of ship propulsion again into the focus of engineering. In 2010 a new ship the Enercon E-Ship 1 was tested, providing four Flettner-rotors as additional propulsive device.

Besides the application of rotating cylinders in a rotor ship, several concepts for lifting devices were studied and tested in flight. The most important aircraft in this context are the rotor airplane A-A-2004 built in 1929 by the Plymouth Development Corporation near Mamaroneck N.Y., and the OV-10 Bronco converted by NASA in 1972 with a rotating cylinder integrated in the leading edge of the flaps.

3.1. Ships

A chapter about ships seems inappropriate in a paper about aeronautics, especially because the Magnus effect was used for propelling a ship rather than for lifting an airplane. However, rotor ships have been the first large scale Magnus effect applications for commercial purposes. Furthermore, the rotor ship is the only product using Flettner-rotors which is documented in detail. Last but not least, the story of Flettner's rotor ship is a prime example for the way to go from pure scientific research to a successful application.

Flettner's rotor project was faced with skepticism about the practical use of a rotating cylinder [10]. Questions like "What would happen in a hurricane since the rotor sails cannot be shortened like the conventional sails?" or "How to deal with vibrations forced by the rotating cylinders?" could not be answered satisfactorily, before tests were conducted.

But Flettner was convinced that the rotor ship would replace all sailing ships in the future and filed a German Patent in 1923 [38], which was also protected in the United States in 1928 [36].

3.1.1. Rotor ship *Buckau*

The first prototype of a rotor ship was a converted schooner, built in 1920 by the German *Germania Werft*. Anton Flettner intended to replace its fabric sails by rigid sails, not only for aerodynamic reasons. His previous innovation, the *control rudder*, was a very successful hydrodynamic control device which could be deflected by minimal forces and which was in fact a rudder for a rudder. Flettner's idea was to build a rigid sail similar to his patented rudder, which looks like a vertical wing and is easy to handle. His brother Andreas Flettner told him by chance about recent experiments at Göttingen which were conducted by

¹ Patent research for International Patent Classification B64C 23/08 *Magnus effect*.

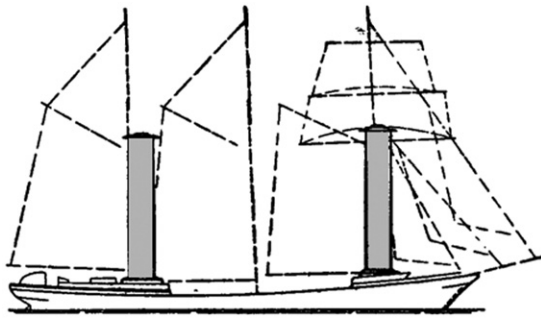


Fig. 32. Side view of *Buckau's* sails and rotor arrangement (rotor marked in grey). Adapted from source: [10].

Table 1
Technical data of rotor ship *Buckau* [12,139].

Total sail area (m ²)	883
Total rotor area (m ²)	87.4
Rotor diameter (m)	2.8
Rotor height (m)	15.6
Rotor weight (to)	7
Max rotor rpm (min ⁻¹)	135
E-motor power (kW)	2 × 11
Max speed (kts)	9.1

Ludwig Prandtl and his research group. When he heard that in these experiments aerodynamic force coefficients on a rotating cylinder were measured which were ten times higher than on a sail of equal reference area, he stopped all activity on the *Buckau* conversion. His project manager and chief engineer Heinrich Croseck, employee of *Flettner Schiffsruder GmbH*, was directed to change the layout and to convert the *Buckau* to a rotor ship. After its conversion, the total rotor area comprised only a tenth of its initial sail area, 88 m² (Fig. 32).

Some technical data of the rotor ship *Buckau* can be found in Table 1. Both cylinders, made of zinc coated sheet steel with a thickness of 1–1.5 mm, were mounted on slide bearings at the pivots, where a lubrication circuit supplied the oil. An electrical system was installed, comprising an electric generator driven by a diesel motor, and two electric motors to drive the cylinders (220 V, 15 hp each). The main engine and one screw propeller still served as primary propulsion system. Flettner proposed to use the Magnus effect not as sole but as additional source for propulsion, to reduce fuel consumption [12].

The independent studies of Prandtl's institute, which revealed the effect of endplates on rotating cylinders, and the skills of Croseck were fundamental contributions to the technical success of the first rotor ship. However, Flettner clearly was the only person, who saw the advantages for ship propulsion [60].

The rotor ship, renamed to *Baden–Baden*, made only one trip across the Atlantic Ocean (Fig. 33). On its 6,100 miles route to New York, the Cape Verde Islands were passed heading south to test the ship in the trade winds. After arrival in New York, Flettner presented the rotor ship to potential customers, but failed to sell it. One reason was probably the long investment depreciation period caused by the low fuel price. The rotor ship was damaged by a lightning strike during one of several presentations along the east coast.

Concerning an application of a Flettner-rotor, it can be concluded that a rotor ship with an auxiliary engine exhibits operational advantages compared to a sailing ship with an auxiliary engine. There are fewer crew members required, the rotor ship can sail to within 20–30° of the wind instead of 45° with conventional sailing ships and very small heeling (less than 5°) was observed during tests under severe weather conditions

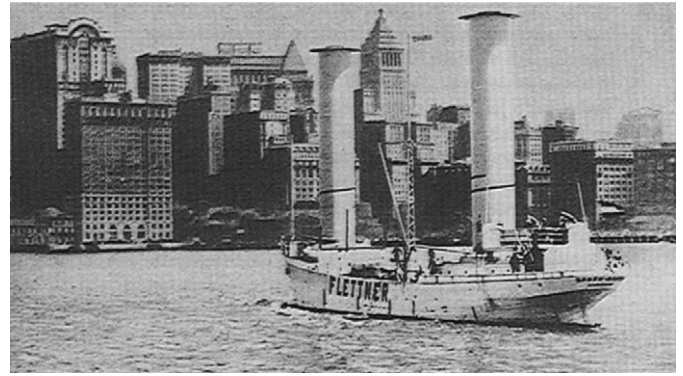


Fig. 33. Arrival of the rotor ship *Baden-Baden* in New York (05/10/1926), picture: Berliner Illustri(e)rt.

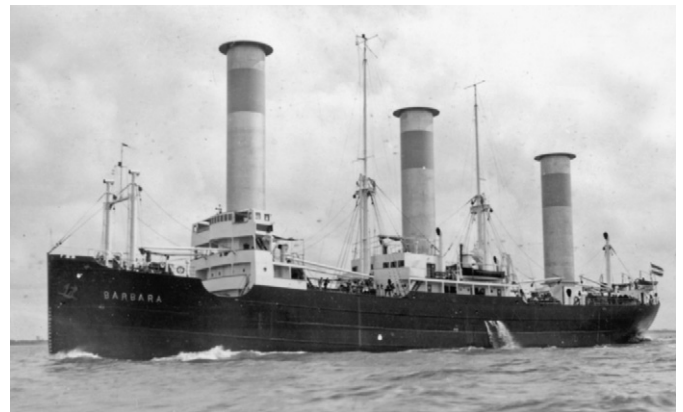


Fig. 34. Rotor ship *Barbara*. Courtesy of Deutsches Schifffahrtsmuseum Archiv, Bremerhaven.

Table 2
Technical data of rotor ship *Barbara* [139].

Rotor area (m ²)	204
Rotor diameter (m)	4
Rotor height (m)	17
Max rotor rpm (min ⁻¹)	150
Diesel motor (PS)	2 × 530
E-motor power (PS)	3 × 35
Max speed (kts)	13

[10,12]. The previous skepticism about the claims for high efficiency of the rotors as well as handling and seaworthiness, expressed in 1924 [71], was disproved.

3.1.2. Rotor ship *Barbara*

The cargo ship *Barbara*, built in 1926 for the shipping company Rob. M. Sloman, was the second rotor ship equipped with Flettner-rotors and therefore was the first motor ship with an additional wind propulsion system (Fig. 34), compared to *Buckau*, which was a converted schooner.

The construction of these Flettner-rotors and their driving system was similar to those of rotor ship *Buckau* with some improvements. Instead of slide bearings, ball bearings were used for the pivots. Lightweight material aluminum was preferred for the rotor construction. More technical data can be found in Table 2.

During the six-month test phase, Captain Lohmann and the inspector of the ship owning company *Bruno Richter* found that

the rotors produced an additional power of 600 hp at wind speeds of 6 Beaufort (equals 11–14 m/s). Test rides at 4–6 Beaufort led to a top speed of 13 kts when both combustion motors were running at full power. One motor combined with the rotors operative, propelled the ship up to a speed of 10 kts. The rotors alone pushed the ship to a speed of 6 kts. The rotors were operative during 30–40% of the duration of the trip and increased the top speed about 2–3 kts. The fuel consumption per rotor is stated as 1 kg/h, which is very low for the additional power mentioned above.

Over six years of operation, mainly in the Mediterranean Sea, the functionality and reliability of the Flettner-rotor system was proven. The rotors kept in good condition, even at adverse weather conditions with wind speeds up to 12 Beaufort.

3.2. Aircraft

There have been many ideas on how to use the Magnus effect in aeronautics, as presented before in Section 1.3. Obviously, there must have been some prospective advantages compared to conventional airplane. Otherwise airplanes which use the Magnus effect would not have been built in the past.

As demonstrated with the rotor ship *Buckau*, a very high lift coefficient could be attained by a Flettner-rotor. This characteristic was considered to be useful either for an aircraft configuration with high wing-loading or for attaining a low landing speed [72].

It is an interesting fact that all rotor airplanes ever built comprise a conventional fuselage with a conventional tail and standard control surfaces. There was the opinion that a replacement of the wing by a rotating cylinder is all that is necessary to achieve a good rotor airplane design. Difficulties in handling the expected gyroscopic forces were apparently not encountered, except on the Plymouth A-A-2004 airplane.

It has to be mentioned that after the first presentation of *Buckau* to the public in 1924 Flettner's rotor ship triggered many discussions about the application of Flettner-rotors to airplanes. It was commonly thought that vibrations, drag, weight and cost would prevent the use of the Magnus effect. In addition, the Treaty of Versailles, signed at the end of World War I in 1919 and in force until 1933, inhibited any development of aircraft in Germany. Little work was undertaken in Europe on Magnus rotors as lifting devices for air vehicles, but in the United States of America experimental rotor airplanes were built and tested.

3.2.1. Rotor airplanes

An aircraft, which uses the Magnus effect by a rotating cylinder defines a new category besides fixed wing and rotary wing aircraft. This new category is justified by the aerodynamics of the lifting device as well as the flight mechanics such as stability and control. In this section rotor airplanes are presented, which were built in the past.

3.2.1.1. Butler Ames Aerocycle. The first report on rotor airplane activities appeared in the newspaper *Evening Sun*, dated 23th of July, 1910 [73], seven years after the Wright brothers' first flight. According to this report, the new aircraft *Aerocycle* was tested on the destroyer USS *Bagley* [74]. This aircraft was designed by Congressman Butler Ames during July and August 1910 [73]. The aircraft was assembled and tested on a platform behind the bridge (Fig. 35). Butler Ames used this testing platform for 11 day for his aircraft in an experiment trying to create lift from rotating barrel-forms, powered by a 40 hp Curtiss V-8 [75]. There is no record about an actual flight.

3.2.1.2. Plymouth A-A-2004. In the 1920s it was a common opinion that the rotating cylinder could not replace airplane



Fig. 35. Two drum wings with endplates mounted side-by-side on top of the torpedo boat, picture: *Evening Sun*.

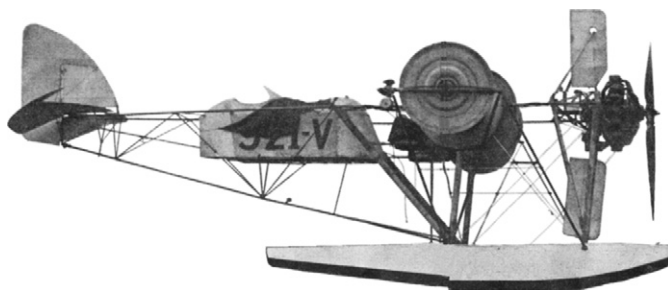


Fig. 36. Plymouth A-A-2004. Courtesy of Deutsches Museum Archiv.

wings, as they were not regarded as being cost-effective [12]. On the other hand, some regarded the static wing as having reached a developmental dead end, and that the rotating cylinder represented the radical innovation that would enable aircraft development to proceed [76]. A wingless aircraft, an aeronautical application of the Flettner rotor ship, was developed by three inventors on Long Island Sound off Mamaroneck NY (Fig. 36). In 1930, short flights were reported in newspapers [77,78] and magazines [34,79,80].

This full size rotor airplane was propelled by a standard airplane engine and its three-bladed propeller. An auxiliary four-cylinder air-cooled engine spun three spool-like cylinders with a diameter of 2 ft. In addition to a conventional tail, unique vertical control surfaces were mounted near the front of the fuselage. Their intended purpose probably was for roll control instead of standard wing ailerons.

Several pairs of floats from Edo Manufacturing Company had been used, and one was badly damaged in a rough landing. The floats were attached by V-struts to the outer ends of rotor axles in addition to the usual mounting.

Zaparka [81–86], the owner of this rotor airplane, filed six patent applications for Magnus effect devices. His inventions were in the field of lifting devices and flight control devices for rotor airplanes. Besides problems in flight control, structural strength was a major issue to be solved for this type of vehicle [77]. Aircraft registration data is taken from [87], and is presented in Table 3.

3.2.1.3. Union aircraft. Two years later, in 1931, another rotor airplane was built by the Union Aircraft Corporation in Long Island NY (Fig. 37). It was designed and constructed by Isaac C. Popper and John B. Guest.

Table 3
Aircraft registration of Plymouth A-A-2004, 921V.
Source: [87].

Aircraft registration (V)	921
Model	A-A-2004
Make	Plymouth
Manufacturing date	1929
Engine	Wright R-540-A, 165 hp
Rotor engine	American Cirrus, 90 hp
License application	3/4/30
Manufacturer	Plymouth Development Corp. 230 Park Ave. New York
Builder/Owner	E.F. Zap.
Dated 11/28/32	Zap Development Corp. Baltimore, MD

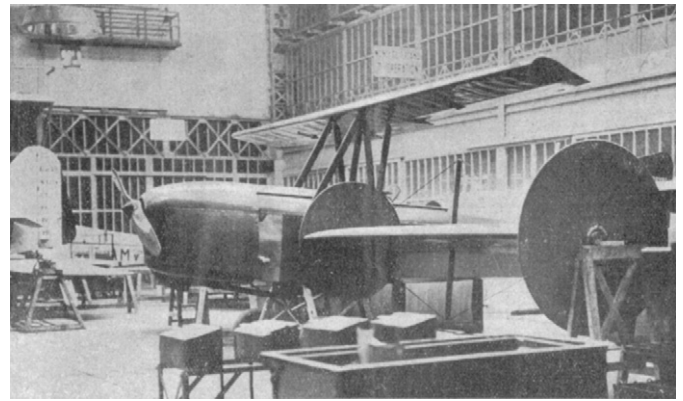


Fig. 38. Autogyro of Chappedelaine. Courtesy of Deutsches Museum Archiv.



Fig. 37. Union Aircraft X772N. Courtesy of Deutsches Museum Archiv.

Table 4
Aircraft registration data of Union Aircraft X772N.

Aircraft registration	X772N
Manufacturing date	1931
Engine	American Cirrus, 90 hp
Rotor engine	2 × Indian, 28 hp
Manufacturer	Union Aircraft Corporation Long Island, NY

Four conical spindles in an open frame replaced the wings and were driven by two additional 28 hp Indian (motorcycle) engines. The two large rotors in front produced lift and the small rotors acted as stabilizer. A landing speed between 5 and 10 mph was estimated by Popper. More technical data can be found in Table 4. The rotor airplane was an experiment to create lift based on the Magnus effect. Although the designer claimed it had double the lifting power of conventional wings and could land at half the speed, there is no record of actual flight.

3.2.2. Autogyro of Chappedelaine

An autogyro is an airplane with rotating wings. Two different types of autogyros are well known, distinguished by the vertical or horizontal rotational axis of the wings or blades, respectively. The autogyro of the French citizen Jean Louis de Chappedelaine is a hybrid configuration, consisting of a rotatable wing and a conventional fixed wing in a biplane arrangement (Fig. 38).

This airplane is specified in a patent filed in Great Britain [88]. The inventor describes the rotatable wing as an S-shaped rectangular wing, which enters auto-rotation about its rotational axis under the action of air resistance. A ratchet wheel ensures the correct direction of rotation. The purpose of this rotatable wing was to generate very high lift forces and consequently to take-off and land at very steep angles and at very slow speed. The rotation of the wing could be stopped with brakes and its position could be

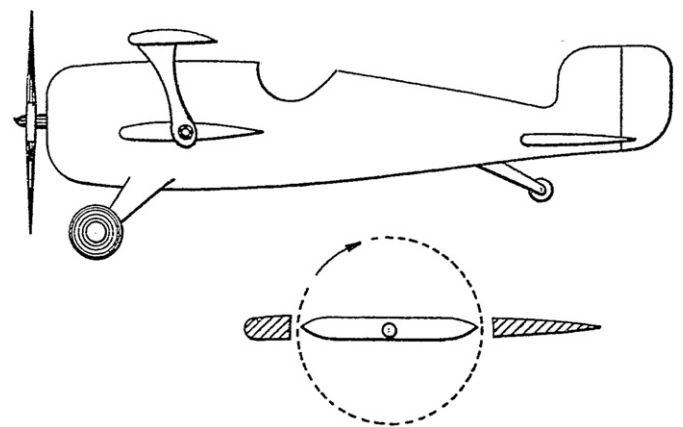


Fig. 39. Sketch of a biplane with a fixed wing in the upper position and a rotating wing in the lower position [88].

locked in such a manner as to permit the machine to be used as an airplane with fixed wings (Fig. 39).

The lateral control of the airplane was to be ensured by the differential action exerted by the pilot on the speed of rotation of the wings by means of suitable brakes. Furthermore, the upper fixed wing carried ailerons, which were to be used as in ordinary aircraft.

This autogyro does not use the Magnus effect, as the rotor airplanes above, by affecting the boundary layer through a spinning cylinder, but the technical details could be taken as suggestion to other rotor airplanes with respect to flight control. This configuration can be related to the biplane of Wilke (compare to Fig. 8).

3.2.3. Test aircraft NASA YOYV-10

This STOL aircraft is equipped with a conventional wing for lift generation and an additional Magnus effect device to improve the high lift aerodynamics. In contrast to the other rotor airplanes mentioned above, a large amount of data and results provide insight into the performance and dynamics of such a Magnus effect device in flight.

Beginning in 1972, NASA used the third YOYV-10A prototype to test high-lift systems, including a rotating cylinder flap concept, proposed by Calderon [21,89], to drastically increase low-speed performance. This concept included a large hydraulically-spun rotating cylinder at the leading edge of a Fowler flap, as described by Cichy [22]. Two Lycoming T53-L-11 turboprop engines,

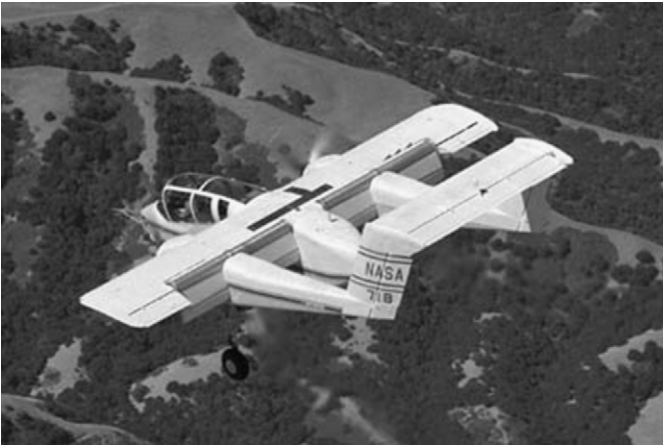


Fig. 40. Modified YOY-10A prototype with an integrated rotating cylinder flap, registered N718NA. Courtesy of NASA.

producing more than 1,000 shp each, were fitted with 4-bladed 10 ft diameter composite propellers. Both engines were interconnected by a driveshaft for safety reasons in case of an engine failure. The aircraft had a short 34-ft wing (Fig. 40).

The rotating cylinder concept as proposed by Calderon is a boundary layer control device. Four cylinder segments were integrated in the leading edge of a Fowler flap. They had end disks of 14.4 in (inboard) and 16.8 in (outboard). The cylinder itself had a diameter of 12 in. The cylinder speed was set at 7500 rpm during flight. Wind tunnel tests of this aircraft configuration indicated that this cylinder rpm would provide flow attachment for a 90° flap deflection at speeds up to 70 kts. Total power required to drive the four cylinder segments at this rpm was approximately 30 hp. In conjunction with a propeller slipstream, this device produced lift and drag characteristics required by STOL vehicles for steep approaches and short landings. Furthermore, an improved turning effectiveness was expected. The characteristics of such a high-lift device are described in more detail in Section 3.3.1.

Experiments were conducted in the Ames 40 by 80 ft wind tunnel, with a model equipped with a rotating cylinder flap, either with two propellers [90] or four propellers [91], providing approximately the same slipstream coverage on the wing. The test results revealed that large lift gains were obtained for the four-propeller configuration, as a result of the larger ratio between the affected flap span and propeller diameter. The required velocity ratio u/V for attached flow turned out to be dependent on flap deflection only. It was independent of angle of attack, propeller slipstream effects, and wing tilt. This investigation included an examination of the effects of cylinder speed, propeller thrust, nacelle spacing, wing leading-edge slats, wing and nacelle tilt, fuselage strakes, and horizontal tail location on flap effectiveness, stall characteristics, longitudinal stability, slipstream turning, and descent characteristics.

The correlation of these wind tunnel results with flight test results was investigated by Cook [92]. The airplane lift coefficients obtained in flight generally exceeded the initial estimates and values obtained in full-scale tunnel tests. An unexpected shift in pitching moment characteristics, which required full nose-down control at low speeds, was not predicted from full scale wind tunnel testing. The full-scale wind tunnel test downwash values were lower than either the flight data or estimates.

Lateral-directional dynamic stability in flight was dominated by an unstable spiral mode, which was apparent in the low values of dihedral effect from the wind tunnel data. Furthermore, Dutch roll frequencies and damping were lower than estimated [22]. A total of 34 flights were conducted and described in [22,93]. The flight test

results indicated that landings could be made with approach speeds of 55–65 kts (corresponds to $C_L=4.5$) and descent angles of 6–8° for total flap angles of 60–75°. Landings with flap deflections greater than 75° were not attempted because of unstable pitch characteristics, low longitudinal control margins, low directional stability, and even lateral instability. Stall approaches were characterized by directional wandering and tendency to diverge at low sideslip angles ($\pm 5^\circ$); 0° sideslip was difficult to maintain. Approach to the stall at high flap angles was accompanied by buffet and vibration, pitch up tendency, and reduced pitch control.

The biggest contribution to pilot workload was probably the lateral axis. The aircraft was easily disturbed in turbulence and although sideslip excursions did not seem very large, the roll motion was objectionable. The aircraft could fly at 47 kts, but became directionally unstable near 30 kts. Small modifications were made to improve the low-speed handling qualities. A differential propeller blade angle system for lateral control power augmentation was flight tested, which gave some indication of reduction in adverse yaw in rolling maneuvers. An increase in horizontal tail incidence angle was necessary to lessen the possibility of tail stall.

The pilot commented that glide slope tracking was not too bad, but it seemed more difficult to correct from a low approach than from a high. The pilot had the impression that flare capability might be quite sensitive to airspeed at flare initiation. But none of the landings were uncomfortable.

Takeoffs were made with 30–45° flap setting. The take off speeds were 75–80 kts with climb angles of 4–8° depending on power setting. Calculated total takeoff distance over 50 ft was approximately 1200 ft.

A failure of a powered lift system is a safety issue, even for the Calderon system. The failure of a cylinder drive system was simulated without any problem due to the long run-down time of the cylinders. The conclusion was that a sudden aerodynamic change is avoided by the angular momentum of the rotating cylinders which provides enough time for the pilot to react properly. A single engine failure was also simulated satisfactorily.

Noise measurements were made by flying the airplane at constant 70 kts airspeed and 50 ft altitude over an arrangement of microphones set up on the runway. The noise level on the ground under an 8° landing approach path was below 86 PNdB at distances beyond one nautical mile from touchdown.

These experiments demonstrated on the one hand the effectiveness of such a high lift system but on the other hand the weakness in handling qualities due to the gyroscopic forces in such an aircraft configuration.

3.2.4. Lighter-than-air system

The Magenn Air Rotor System MARS™ is a lighter-than-air tethered wind turbine that rotates about a horizontal axis in a wind stream to generate renewable electrical energy. This electrical energy is transferred down the 1000-ft tether for immediate use, or to a set of batteries for later use, or to a power grid. The Helium filled MARS allows it to ascend to various altitudes. A three-bladed prototype with 10–25 kW power output is shown in Fig. 41 and a former 10 kW proof of concept in Fig. 42.

MARS captures the energy available in airstreams at 600–1000-ft altitudes. In addition to power generation, the MARS rotation also generates the Magnus effect, which provides additional lift, keeps the MARS stabilized, and positions it within a controlled location.

This wind turbine system is mobile and can be rapidly deployed, deflated, and redeployed without the need for towers or heavy cranes. It is bird and bat friendly with low noise emissions and is capable of operating in a wide range of wind speeds from 4 mph to greater than 60 mph.

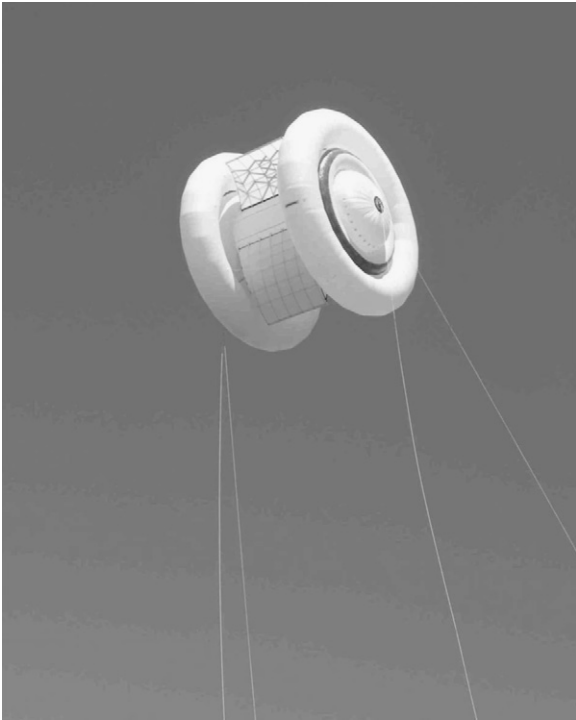


Fig. 41. MARS 10–25 kW prototype in 2009, reprinted with permission from Magenn Power Inc.



Fig. 42. MARS 10kW proof of concept in April 2008, reprinted with permission from Magenn Power Inc.

MARS' performance data are given in Table 5.

3.3. Magnus effect devices

Magnus effect devices are defined as power assisted high-lift systems where a moving wall, e.g., a rotating cylinder, affects the boundary layer of an aerodynamic device. Blowing or suction systems are not considered here.

3.3.1. Boundary layer control by a rotating cylinder integrated in an airfoil

The purpose of a boundary layer control device is to increase lift and to delay the stall angle. A moving surface attempts to accomplish this in two ways. It prevents the initial growth of the

Table 5

Performance specification of MARS 100 kW.
Source: Magenn Power Inc.

Diameter (ft)	45
Length (ft)	100ft
Helium volume (ft ³)	200,000
Tether height	750 ft (max 1500 ft)
Start-up wind speed (m/s)	2.5
Maximum wind speed (m/s)	30
Life cycle (years)	10–15

boundary layer by minimizing relative motion between the surface and the free stream, and it injects momentum into the existing boundary layer. Depending on the performance required, appropriate combinations of cylinder location and rotational speed can be selected to obtain favorable results over a wide angle of attack range.

Early lift and drag coefficient investigations of a wing with a rotating cylinder integrated in the leading edge were done by Wolff and Koning [94,95]. The rotation of the cylinder had a remarkable effect on the aerodynamic properties of the wing. Observations were made in the wind tunnel on how the lift at different wind velocities was affected by rotating this integrated cylinder. The major objective was to find an airfoil-cylinder combination suitable for maintaining safe flight in the event of cylinder stoppage.

Tennant et al. [96] reported circulation control for a symmetrical airfoil with a rotating cylinder at its truncated trailing edge. The lift coefficient was found to be a linear function of the velocity ratio $\alpha = u/V$. For zero angle of attack, a lift coefficient of $C_L = 1.2$ was attained at $\alpha = 3$. Also of interest is the study of Tennant et al. [97,98] concerning the boundary-layer growth on moving surfaces accounting for gap effects. An analytical model based on the method of Cebeci and Smith for the region of flow from the fixed wall (wing) through the transition region gap and onto the moving surface (cylinder) showed good correlation with experimental data.

An assessment of the relative merit of the moving surface boundary layer control (MSBC) with other procedures for boundary-layer control such as suction, blowing, etc., would be of interest. But few results permitting rational comparison have been reported in the literature. However, a few general observations can be reviewed here.

One of the attractive features of MSBC is the negligible amount of power involved in driving the cylinders. Essentially it corresponds to the bearing friction and the torque resulting from the skin friction of the rotating cylinder. Modi gives an example where he compared the case of boundary-layer control by suction with the case of MSBC [58]. Total suction power as applied to a typical airplane with a total weight of 4500 kg and a wing area of 23 m² required about 15–35 hp, depending on the system used. In this case, the lift coefficient was raised from 0.87 to 1.5 and maximum AoA from 10.5 to 15°. On the other hand, North American Rockwell's YOY-10A has similar characteristics, with a total weight around 4500 kg and a wing area of approximately 27 m². The lift coefficient was raised to 4.5, whereas the power required to drive the cylinder did not exceed 30 hp, as mentioned above (Section 3.2.3). In this operational range, MSBC is three times as efficient as the application of the boundary layer suction concept.

Calderon and Arnold [21] carried out tests on a rotating cylinder flap to evolve a high-lift airfoil for STOL-type aircraft. The system was flight tested on a single-engine, high-wing research aircraft designed by the Aeronautics Division of the Universidad Nacional de Ingenieria in Lima, Peru. The advantages

of such a high-lift device are large gains in flap lift with low rotating cylinder power, low longitudinal trim requirements, and low flap hinge moments.

On the basis of Calderon's encouraging results of small-scale tests an investigation was made of the rotating cylinder flap principle applied to a large twin-engine turbo-propeller airplane (see Section 3.2.3). Details of the flap are shown in Fig. 43.

Wind tunnel experiments of the rotating cylinder flap, which was fitted to the Test Aircraft NASA YOY-10, were conducted by Weiberg et al. [90,91]. With the cylinder rotating, airflow on the flap was strongly attached and insensitive to exterior effects such as slat deflection, propeller slipstream, or surface disturbances ahead of the cylinder. At low velocity ratios, the flow over the surface of the flap is separated. As cylinder speed is increased, the separated area on the flap is reduced. The power required to rotate the cylinders was nearly proportional to the cube of rpm. For a flap deflection of 60° at 40 kts, approximately 0.7 hp per foot of cylinder length was required for flow attachment. The magnitude of the flow induced pitching moment was relatively small, compared to a blowing boundary layer control device [90]. The pitching moment could be reduced by mounting the flap hinge slightly higher (0.11c) than illustrated in Fig. 43 (0.03c).

Another experimental investigation was conducted by Al-Garni et al. [99] based on a NACA 0024 airfoil equipped with a leading-edge rotating cylinder and a flap, see Fig. 44. A parameter study included variation of rotational speed and flap deflection angles. Smoke-wire flow visualization results were used to demonstrate the strong effect of the leading-edge rotating cylinder on the size of the recirculation region. Measurements were conducted at a free stream velocity of 5 m/s and the rotational cylinder speed was varied between 0 and 14,400 rpm.

When the cylinder rotates, a new circulation is induced around the typical circulation about a conventional airfoil without affecting the drag as long as the angle of attack is small. Fig. 45 shows the lift and drag coefficients and the resulting L/D values plotted against angle of attack for different cylinder rotation speeds U_c . With increasing velocity ratio U_c/U , the lift and drag coefficients increase as well, but the slope of the lift coefficient curve remains nearly unaffected. A velocity ratio of $U_c/U=4$

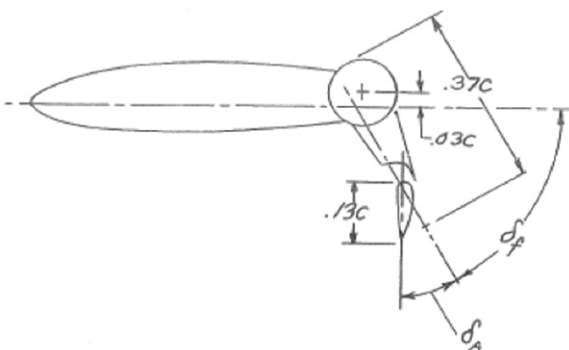


Fig. 43. Rotating Cylinder Flap as proposed by Calderon [22].

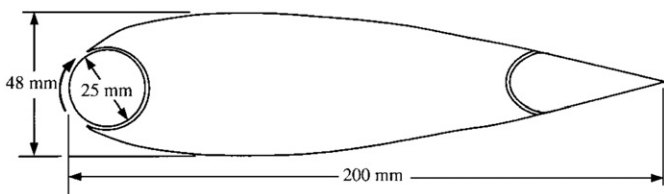


Fig. 44. Rotating cylinder mounted in the leading edge [99], reprinted with permission from AIAA.

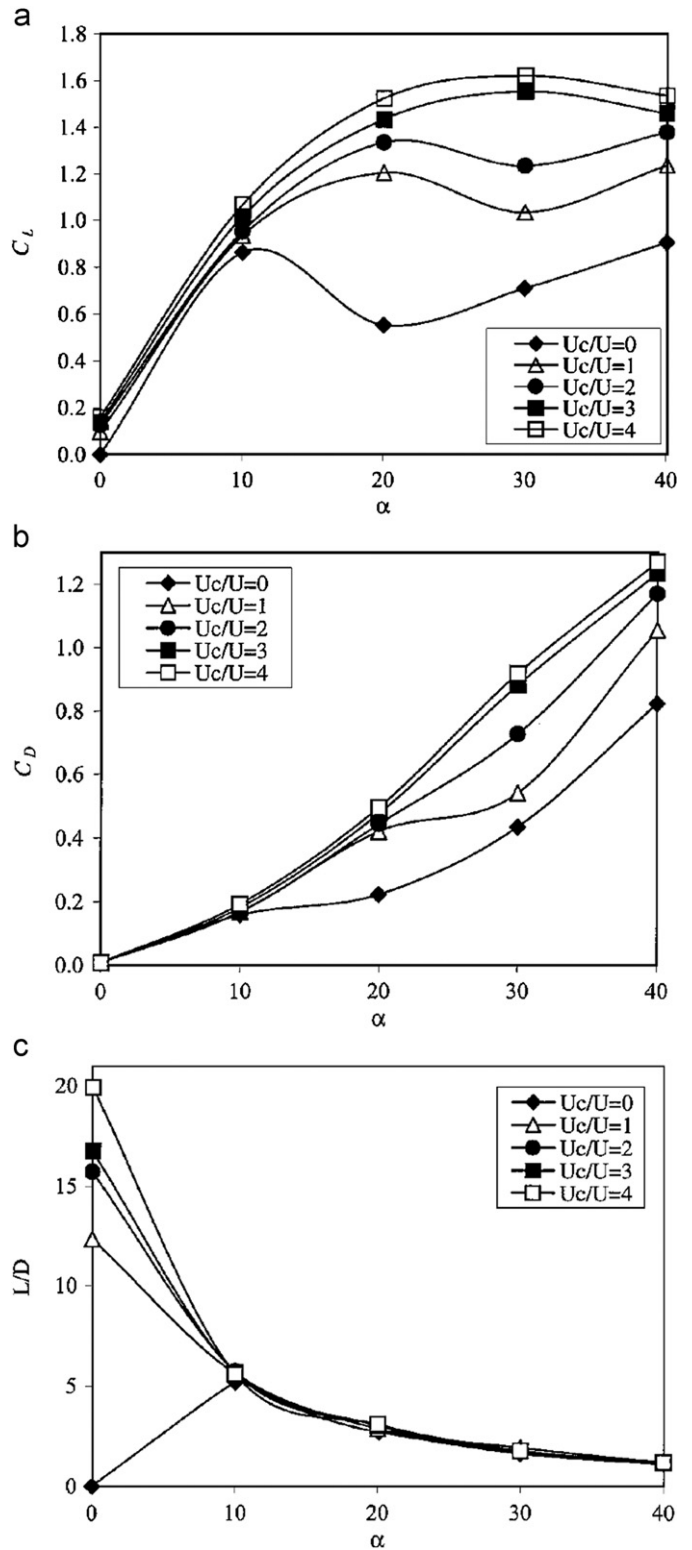


Fig. 45. Effect of leading edge rotating cylinder at $\delta=0^\circ$ on (a) lift coefficient C_L , (b) drag coefficient C_D and (c) lift-to-drag ratio L/D [99], reprinted with permission from AIAA.

results in a maximum efficiency value of around $L/D=20$ for zero angle of attack.

The lift characteristic of an airfoil equipped with a leading-edge rotating cylinder can be greatly enhanced by the use of additional high-lift devices such as a flap. Fig. 46 summarizes the

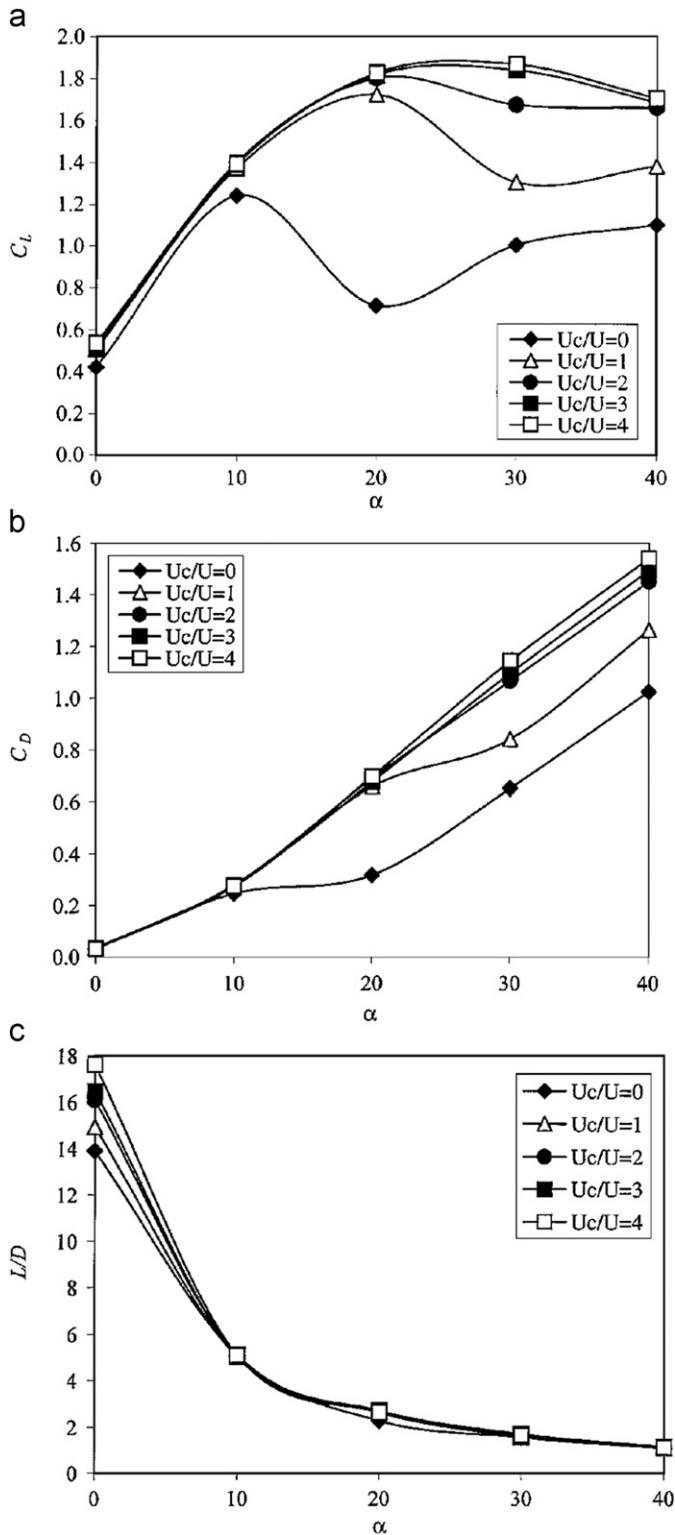


Fig. 46. Effect of an additional plain flap at $\delta=30^\circ$ on (a) lift coefficient C_L , (b) drag coefficient C_D and (c) lift-to-drag ratio L/D . Ref. [99], reprinted with permission from AIAA.

effects of an additional plain flap deflected at $\delta=30^\circ$. The highest lift coefficient with the flap deflected and the cylinder stationary is $C_L=1.24$. This value increases to 1.93 when the cylinder is rotated at $\alpha=4$. Note that the deflection of the flap resulted in a reduction of the L/D ratio of the airfoil by about 10% for $\text{AoA}=0^\circ$ (compared with Fig. 45c).

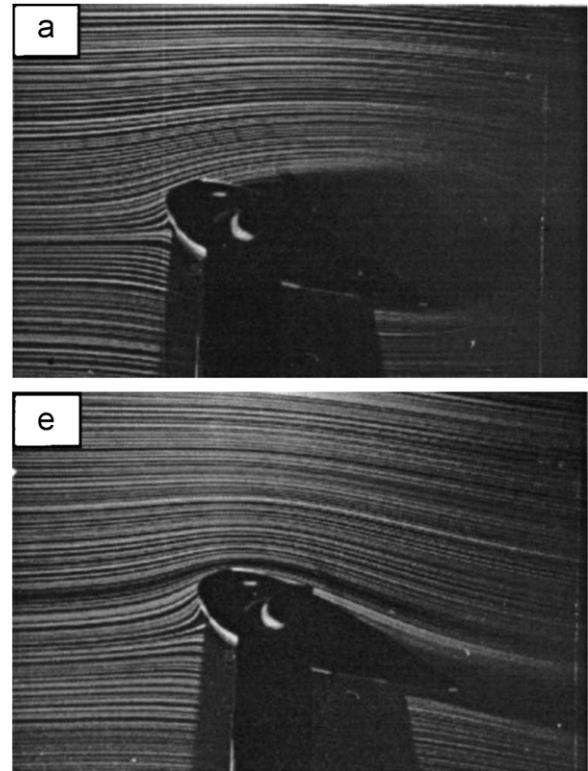


Fig. 47. Flow visualization photographs at 20° angle of attack, (a) $u/V=0$ and (e) $u/V=4$. Ref. [99], reprinted with permission from AIAA.

Flow visualization photographs shown in Fig. 47 give an image of the flow conditions that exist on the upper surface of the airfoil at $\text{AoA}=20^\circ$. At a velocity ratio $\alpha=0$ one can see that the flow over the upper surface of the airfoil is totally separated. However, with the cylinder rotating at $\alpha=4$, the flow becomes reattached.

Al-Garni received a patent in 2002 for a movable surface plane [100]. He recommended that movable endless surfaces over the majority of both sides of the wings shall be used individually for boundary layer control.

Modi et al. compared the distinctive features of different configurations to establish their relative merits. Fig. 48 shows a family of two-dimensional airfoils based on the Joukowski airfoil (15% thickness) with different positions of the rotating elements used to inject momentum [101,102]. The leading-edge cylinder is quite effective in extending the lift curve, without significantly changing its slope. Further improvements in the maximum lift coefficient ($C_{Lmax}=2.73$) and stall angle are possible if the leading-edge cylinder is used in conjunction with an upper surface cylinder. This configuration also results in a lower drag due to a large pressure recovery near the trailing edge at moderately high angles of attack.

A rotating cylinder on the upper side has a major advantage in terms of mechanical simplicity. However, the maximum lift coefficient is slightly lower ($C_{Lmax}=2.35$). Note that the lift curve now has a lower slope and the stall is delayed to approximately 48° .

To improve the lift capability over the range of low to medium angles of attack ($\text{AoA} < 20^\circ$), the trailing edge cylinder proves much more effective, particularly in conjunction with the leading-edge cylinder.

Modi states that the power required to drive the cylinder is virtually insignificant compared to active blowing or suction for boundary layer control [103].

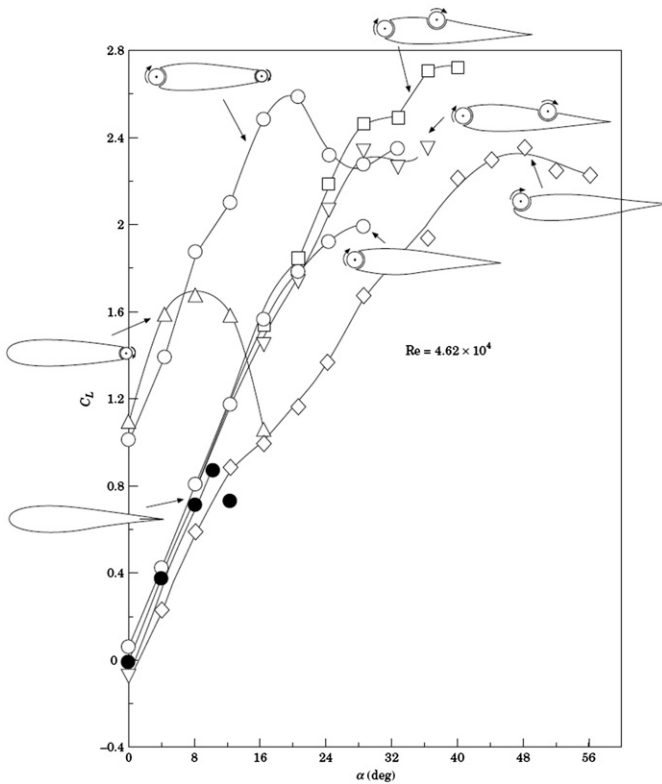


Fig. 48. Plots to assess relative influence of different configurations studied on the lift and stall characteristics. Reprinted from [103] with permission from Elsevier.

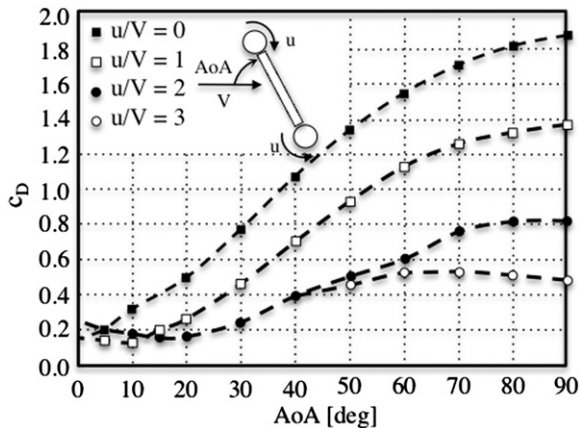


Fig. 49. Plot showing significant reduction in drag of a two-dimensional flat plate with the moving surface boundary-layer control applied at both the leading and trailing edges. Note that at $\text{AoA}=90^\circ$, a reduction in C_D is around 75%. Data according to Ref. [104].

It is interesting to note that rotating cylinders applied to the edges of a flat plate are able to reduce the drag. Modi investigated bluff bodies like a truck and presented a concept to reduce fuel consumption by around 10% at $\alpha=1.5^\circ$ [104]. Fig. 49 shows a significant reduction in drag for a flat plate, depending on the velocity ratio and angle of attack.

Modi summarized the specific characteristics of a symmetrical airfoil using leading- or trailing-edge rotating cylinders in Ref. [105]:

1. In general, rotation of the leading-edge cylinder results in increased suction over the nose. It is the propagation of this lower pressure downstream, however, that determines the

effectiveness of the rotation. This depends mainly on the geometry of the nose and smoothness of transition from the cylinder to the airfoil surface. A large gap substantially decreases the beneficial effect of the cylinder rotation.

2. The increased momentum injection into the boundary layer with an increase in speed of rotation delays the separation of flow from the upper surface (stall) resulting in a higher $C_{L,max}$.
3. With the rotation of the leading-edge cylinder, the onset of flow separation occurs at relatively higher angles of attack. The upper surface flow remains attached up to a distance downstream of the leading edge at which point it separates, leading to a large separation bubble, with reattachment towards the trailing edge. The flow, therefore, is not completely separated from the airfoil, thus resulting in a flatter stall peak.
4. The use of a leading-edge cylinder extends the lift curve without substantially changing its slope, thus considerably increasing the maximum lift coefficient and stall angle. An experimental study with a Joukowski airfoil showed an increase in $C_{L,max}$ by around 130%, with the stall delayed from 10 to 28° .
5. In contrast to a leading-edge cylinder, the use of a trailing-edge cylinder substantially increases the lift before stall. The rotating trailing-edge cylinder acts like a flap shifting the C_L vs AoA plots to the left. A high rate of rotation of this cylinder results in a huge increase in suction over the airfoil upper surface, thus giving a larger lift. Furthermore, it can be used in conjunction with the leading-edge cylinder, resulting in impressive values of lift over the whole range of low to moderately high angles of incidence ($\text{AoA} < 19^\circ$). For both the cylinders rotating at $\alpha=4$, the $C_{L,max}$ increased by around 195%, compared to the unmodified base airfoil.
6. A flow visualization study confirmed effectiveness of the concept and gave better appreciation of the complex flow with a separation bubble and a large turbulent wake. The unsteady flow field is not stable, but oscillates in the stream-wise direction.

The lift to drag ratio for a single- and a two-cylinder case is shown in Fig. 50. The lift and drag data of the modified NACA 63-218 airfoil with an integrated cylinder at the leading edge showed a substantial increase in the lift to drag ratio C_L/C_D at almost all angles of attack. However, for a velocity ratio $Uc/U > 2$, any additional gain appears to be only marginal.

Tests with a model having an additional plain unslotted flap were aimed at assessing its lifting and pitching moment effect. As can be expected, the effect of flap deflection is to shift the lift curve to the left and to increase the $C_{L,max}$ value. It is of interest to recognize that in spite of a large change in lift due to momentum injection, the corresponding change in pitching moment is essentially negligible in the region of $\text{AoA} < 10^\circ$.

Modi's tests also provided useful information concerning the importance of the gap size between the cylinder and the airfoil. In general, an increase in the gap size affected the flow adversely and, for a gap size greater than 4.5 mm, the beneficial effects of cylinder rotation tended to be negligible. For comparison, his wind-tunnel models had an average gap size of 1.5 mm. The power required to rotate the cylinders was always below 50 W [106].

Mokhtarian et al. [107] investigated the effect of the leading-edge geometry. One of the experimental tests was performed with a scooped cylinder given in Fig. 51. The conclusion is that effectiveness of the leading-edge cylinder can be improved at lower speeds of rotation by using a scooped configuration. The rotating air scoop appears to redirect more air over the upper surface. However, at high rates of rotation, it appears to the flow

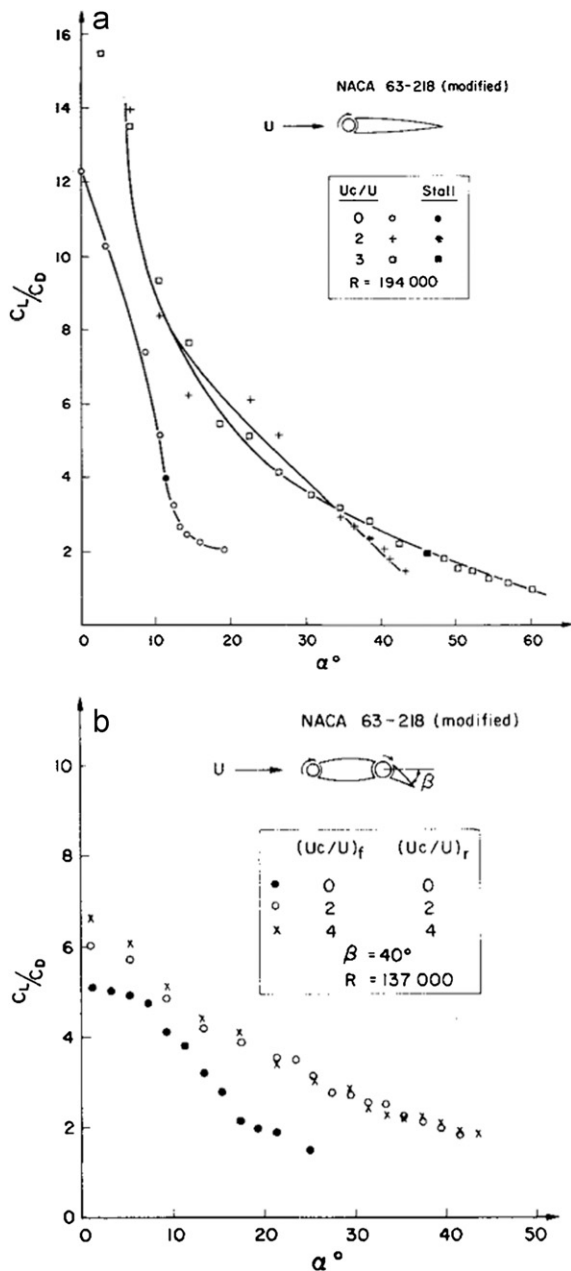


Fig. 50. Effect of cylinder rotation on lift to drag ratio: (a) single cylinder case; (b) cylinders at leading edge of the airfoil and its slotted flap. Ref. [106], reprinted with permission by AIAA.

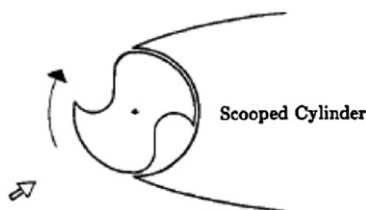


Fig. 51. Symmetrical airfoil with an integrated scooped cylinder. Adapted from source: [107].

effectively as a solid cylinder, and there is no particular advantage in using the scoop configuration.

More recent work was done by Du et al. [108]. The main objective of this study was to measure and characterize the effects of a leading-edge rotating cylinder on the growth,

development, and separation of the boundary layers and wake structures developed on and behind a symmetric airfoil by using hot-wire anemometry and smoke-flow visualization methods. Surface pressure measurements were also made to quantify the variation of lift-to-drag ratio under the influence of cylinder rotation.

Circulation control for a symmetrical airfoil with a rotating cylinder forming its trailing edge was also presented by Tennant et al. [96]. The lift coefficient reached 1.2 with $\alpha=3$ at zero angle of attack. The lift coefficient values and the stagnation point location were found to be linear functions of the cylinder velocity ratio α . In [98,109] the region of transition from a fixed wall to a moving wall was analyzed. Tennant also applied a moving wall to airflow through a diffuser with a step change in area. Experimental results showed no separation for the appropriate velocity ratio [110]. The MSBC concept appears to be quite promising in improving lift capabilities requiring negligible amount of power for its implementation. However, many aspects for a successful integration into full-scale airplanes are not yet explored, for example the effect of icing or wing bending.

3.3.2. Vortex flap

The vortex flap is a trailing edge high-lift device consisting of a mechanically driven spanwise circular cylinder located below and near the trailing edge of the wing and rotating in the sense given in Fig. 52. The rotating cylinder is not used as boundary layer control device for the wing. It is intended to be used as single component of a high lift system which might incorporate additional wing leading edge high-lift devices or other components and features [111].

The total aerodynamic coefficients were calculated based on the area of the wing only, here without the cylinder. Wind tunnel experiments demonstrated the Vortex Flap as the most effective lift-generating single rotating circular cylinder configuration [111]. For example, a Clark Y based Vortex Flap configuration provided a maximum lift coefficient $C_{L,max}=3.65$ compared to the airfoil alone providing only $C_{L,max}=1.19$.

3.3.3. Propulsion

The initial euphoria accompanied by the technical success of Flettner's rotor ship stimulated the creation of a new concept for the propulsion of an airplane, the so called rotor propeller [11]. Such a propeller is based on rotating cylinders, which replace the conventional propeller blades of a propulsion system or wind turbines, respectively. For some reason such a concept has not been developed past the experimental stage. Models have been constructed that work well, proving that the principle is valid. Calculations indicated that the thrust that can be developed by a rotor propeller is 59% higher than that of a screw propeller of similar diameter [24]. A propeller having blades of circular cross-sectional contour has been patented for the inventors Lee and Zaparka [81].

3.3.4. Hybrid rotor

The Hybrid rotor is a new concept for a propulsion and lifting device, which might be used for VTOL aircraft in the future. This solution is able to provide thrust, lift and control power at the same time. It is a two-dimensional propulsion system with 360°



Fig. 52. Basic Vortex Flap Configuration, according to [111].

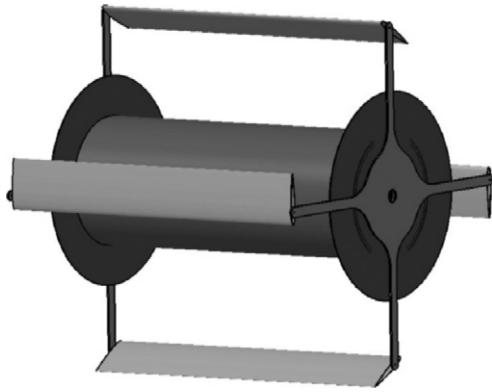


Fig. 53. Schematic view of the Hybrid rotor, providing a cycloidal propeller and an integrated rotating cylinder.

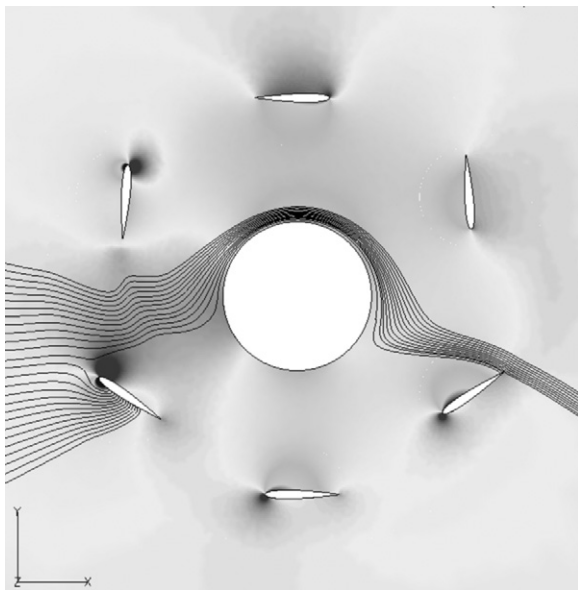


Fig. 54. Flow through the Hybrid rotor (clockwise rotation of cylinder and propeller, air flow from left to right).

thrust vector control. A schematic view is presented in Fig. 53, illustrating the concentric arrangement of a cycloidal propeller and a Flettner-rotor. Aerodynamic analyses were performed to study the flow characteristics and to calculate forces and moments in cruise flight and hovering (Fig. 54). First results are presented and interactions between both rotor subsystems are characterized [112]. Possible advantages and challenges for an application in aeronautics are discussed in [112,113].

The cycloidal propeller and the rotating cylinder are not new in aeronautical applications. However, some important features, benefits and disadvantages of these rotors will be summarized in this section. The cycloidal propeller was studied by various scientists and engineers in USA, Israel, South Korea and Singapore [114–133].

The aerodynamics of a cycloidal propeller compared to the conventional screw propeller is quite different. The uniform distribution of the flow around a cycloidal propeller blade provides high aerodynamic efficiency and low noise. Boschma stated 10.88 lbs/hp compared to a MD-500 Helicopter with 9.45 lbs/hp [118]. Test runs were performed at 550 RPM with a six-bladed cycloidal propeller with 4 ft diameter, which confirmed the quiet operation that was stated before in other reports [119]. But, on the other hand, the unique design of a cycloidal propeller leads to structural and mechanical challenges. The

centrifugal forces combined with the oscillating aerodynamic forces at the propeller blades lead to alternating loads and moments. A stiff and light weight structure and optimum design is required for the propeller blades to compensate these loads [124,125]. The design of the connecting parts, especially the bearings of the propeller blades seem to be a challenging task in order to get them rated for endurance strength. Hwang et al. [133] applied a swash plate to the rotor system to improve the rotor performance and control mechanism. The purpose of using the swash plate is to decrease the whirling of the cantilever shaft by enlarging the shaft diameter, to make the control devices compact, and to be located inside the fuselage. This new mechanism enables easier control of the aircraft, in addition to the performance improvement of converting the flying mode from hovering to forward flight. Furthermore, this control mechanism shows a fast response to a steering input.

The Hybrid rotor is currently under development by Atena Engineering. A small model was presented at the ILA Berlin Airshow in June 2010 [134].

4. Discussion and summary

Basic principles of Magnus effect devices and their applicability in aeronautics are discussed in this section.

4.1. Comparison between wing and rotating cylinder

A rotating cylinder in cross-flow produces aerodynamic forces similar to a wing. However, the characteristics of both lifting devices are different. First of all, the magnitude of the cylinder lift is controlled by the velocity ratio and not by the angle of attack. What is little known is the generation of a negative Magnus force in the critical range of Reynolds number and the velocity ratio. Furthermore, the endplates of a Magnus rotor play an important role. They diminish the pressure equalization at the tips, just like a winglet does. In addition, the rotating surface of the endplate affects the circulation around the rotating cylinder. Bearing in mind that the reference area of a Magnus rotor is defined as $S_{ref}=l \cdot d$, the surface of the lift contributing endplates is not accounted in S_{ref} . For this reason, a comparison between the aerodynamic coefficients of a wing and a Magnus rotor should be questioned if these coefficients are affected by large or fast spinning endplates. However, the lift-to-drag-ratio is a good measurement for comparing the aerodynamic efficiency of both devices.

The aerodynamic efficiency of a wing and a Magnus rotor can be compared in the low-Reynolds-number regime, for an unswept, untapered, low aspect ratio configuration. Marchman tested a low aspect ratio wing at low Reynolds numbers of 70,000–300,000, based on a Wortmann FX-63-137-ESM airfoil. He presented the aerodynamic coefficients for lift, drag and pitching moment and discussed their hysteresis loop at high angles of attack [135]. The maximum efficiency measured for a wing with an aspect ratio $A=8$ is given by $L/D=24$ at an angle of attack $AoA=10^\circ$. For example, a Flettner-rotor with a little higher aspect ratio $A=12.5$ provides a $L/D=12$, at a velocity ratio $\alpha=2.4$ (see Section 2.1.10).

Aerodynamic data for different kinds of Magnus rotors can be found in the literature for low Reynolds numbers. In addition, Magnus force data for bullets in supersonic flow can be found as well, but there is a lack of aerodynamic data for subsonic flow above $Re=10^6$.

Taking the power requirement for spinning a rotor into account, the overall efficiency of a Magnus rotor will probably always be below that of a wing. Furthermore, the high lift forces

of a Magnus rotor will only be useful if the weight of a rotor system together with its propulsion system can come close to that of an equal sized wing.

4.1.1. Stall characteristics

The stall characteristics of a rotating cylinder differ from airfoil stall. The lift breaks down when the rotation of the cylinder stops. This effect applies to a sole rotating cylinder and to a wing with a rotating cylinder integrated in its trailing edge. A similar stall effect happens if the velocity ratio α and the Reynolds number are in the critical range, where the negative Magnus force occurs. Such a stall can be recovered by a higher velocity ratio. The lift of a symmetrical airfoil typically breaks down if the angle of attack is increased above approximately 15° . The lift force of a rotating cylinder is insensitive to angle of attack. The lift vector remains perpendicular to the free stream without changing its magnitude. However, the lift coefficient is dependent on the velocity ratio and is therefore dependent on the airspeed. This correlation has a surprising implication for aeronautics which will be discussed in the next section.

4.1.2. Gust sensitivity in longitudinal motion

The flight behavior of a conventional aircraft is sensitive to gust and wind shear. The dependency of the aerodynamic forces on the dynamic pressure and the correlation between angle of attack and the aerodynamic coefficients is the reason for this sensitivity. In contrast, a rotating cylinder is a lifting device which generates aerodynamic forces independent from its angle of attack.

The testing of Flettner's rotor ship in the 1920s was extensive and revealed reduced sensitivity to gusts or thunderstorms compared to conventional sailing-ships. Only small heeling was reported to occur in adverse weather conditions [10]. Based on the results of the wind tunnel experiments on a rotating cylinder Anton Flettner explained that the aerodynamic force will not increase in a hurricane because the velocity ratio and consequently the aerodynamic coefficients will decrease, compensating the effect of a rising dynamic pressure [10].

The question arises how this phenomenon can be translated to an application in aeronautics. If there is an operating point of a rotating cylinder where the aerodynamic forces are invariant with a change in airspeed, gust and wind shear insensitivity can be expected for a rotor airplane in its longitudinal motion.

In 1924 the *Flight magazine* explained that the lift force of a Flettner-rotor operated at the proper velocity ratio remains constant in a certain speed range [136]. This phenomenon occurs for Magnus effect devices only where the aerodynamic coefficients are dependent on the airspeed. Figs. 55 and 56 show the lift and drag forces acting on a rotating cylinder and on a wing as a function of airspeed [137]. The dimensions of the rotating cylinder were selected according to the rotors of *Buckau*. Note, that the cylinder speed and the

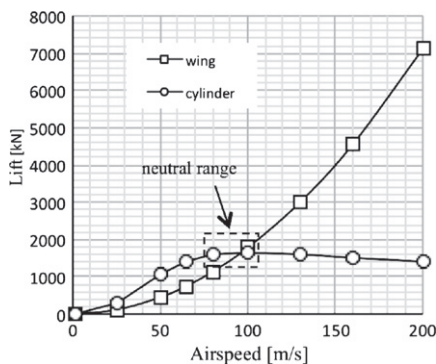


Fig. 55. Comparison of Lift over airspeed for a conventional wing at constant angle of attack and a cylinder rotating at constant speed u .

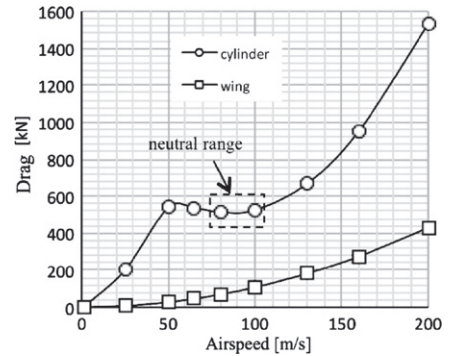


Fig. 56. Comparison of Drag over airspeed for a conventional wing at constant angle of attack and a cylinder rotating at constant speed u .

angle of attack are kept constant. The aerodynamic force on the wing increases quadratically with airspeed. In contrast, the forces on the rotating cylinder are seen to be constant in a certain speed range, called *neutral range*. In this example, the neutral range extends over a range of approximately 30 m/s.

For a Flettner rotor, the neutral range is located where the velocity ratio is between $1.5 < \alpha < 2.0$. It is interesting to note that the maximum aerodynamic efficiency C_L/C_D is close to this α -range (see Fig. 23).

The question arises whether such a favorable behavior in a gusty atmosphere is provided by a similar device, such as a wing equipped with a rotating cylinder in the leading edge. This phenomenon is currently under investigation by the author.

4.2. Recommendations for aircraft conceptual design

Today, there are no specific methods available on how to design the lifting device of a rotor airplane or the rotor airplane airframe. Therefore, the fundamentals of aircraft conceptual design have to be tailored for rotor airplanes. New design methods and charts which show for example the operating points of a rotor airplane during a flight mission are required. Some are presented here.

As mentioned before, the designer has to take care of the negative Magnus force, especially in the case of micro aerial vehicles, because of their flight at low Reynolds numbers, whereas large rotor airplanes are not affected by this phenomenon. With increasing airspeed, the rotational speed is typically reduced to adjust the lift produced at higher dynamic pressure. Below a velocity ratio $\alpha < 0.2$ the negative Magnus force may appear if the Reynolds number is in the critical range between $99k < Re < 501k$. In Fig. 57 the critical flight condition is presented for a MAV where its Magnus rotor has a diameter of 0.1 m. The MAV takes off at an airspeed of 3 m/s and enters the critical range at 20 m/s with a velocity ratio $\alpha < 0.2$.

Flight experiments were conducted with a model of a rotor airplane with a configuration similar to the 921-V described in Section 3.2.1.2. Two rotating cylinders made of sheet of paper with spanwise disks were mounted on top of a commercial slow flyer model (Fig. 58). Its total weight was 50 g and the reference area $S_{ref} = 0.021 \text{ m}^2$. A conventional rudder served for lateral control and a variable cylinder speed for longitudinal control. The flight envelope is within the laminar flow regime. Multiple flights of this model proved the applicability of rotating cylinders to airplanes (see Electronic Annex 1 in the online version of this article). However, many issues such as optimal design and flight control design need further research.

In Fig. 59 a design chart is given, where the rotational speed u and RPM of a Magnus rotor are given versus airspeed V . The rotational speed is indicated in m/s (left ordinate) and rpm (right ordinate). The design chart can be interpreted as follows. The

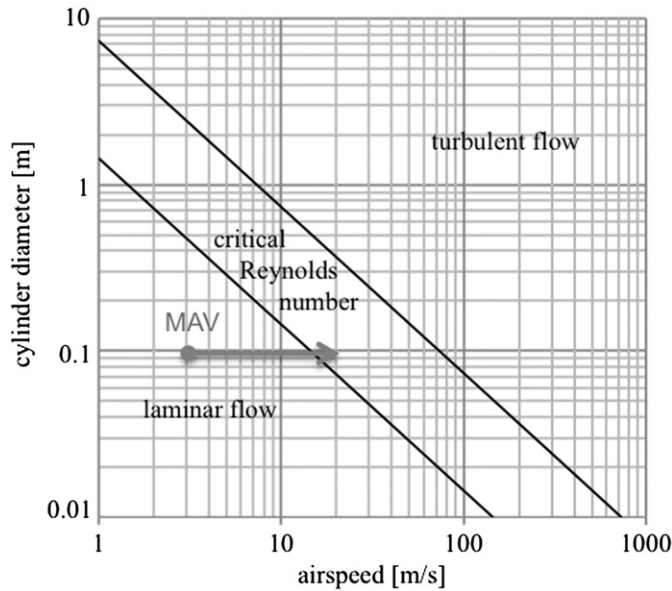


Fig. 57. The Reynolds number is a design driver for MAV with rotating cylinders.

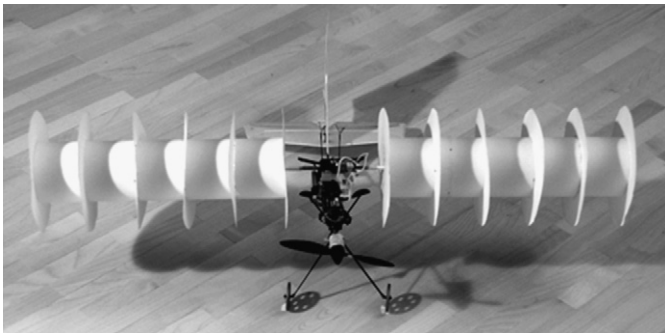


Fig. 58. The authors Remotely Piloted Aircraft based on Thom-rotors.

rotor airplane accelerates from standstill (0) to take off speed with a constant cylinder rate of 7200 rpm. It takes off with a load factor $n_z > 1$ (1). After a short climb segment the flight path levels out with $n_z = 1$. The flight speed increases further from 8 to 50 m/s in horizontal flight, so that the cylinder rate of rotation has to be decreased in order to keep the lift constant (2). The rotor airplane makes then a turn at constant $n_z = 2$ (at a bank angle of 60°) and increases the rotational speed and therefore the velocity ratio to attain more lift (3). Having finished the turn, the rotor airplane levels out at $n_z = 1$ (4). In this way the operating points of the rest of the flight can be interpreted accordingly.

Different velocity ratios from $\alpha = 0.1$ to $\alpha = 8$ are additionally marked in the design chart. These lines of constant α are useful for selecting the design point of a rotor airplane. As example, the design point at maximum lift to drag ratio ($\alpha = 2$) is given in Fig. 59. This chart indicates that an emergency landing with an autorotating Magnus rotor at $\alpha = 0.5$ would be possible with a touch down speed of 24 m/s, if the motor fails to drive the cylinders and a freewheeling mechanism is installed.

Badalamenti and Prince [55] presented power requirements for spinning the cylinder at various endplate sizes. They are shown in Figs. 60 and 61. The lift generated by a rotating cylinder is both rather costly in terms of power required and rapidly reaches a saturation point beyond which no extra benefit in C_L is obtained, regardless of the amount of power input. This is a consequence of the

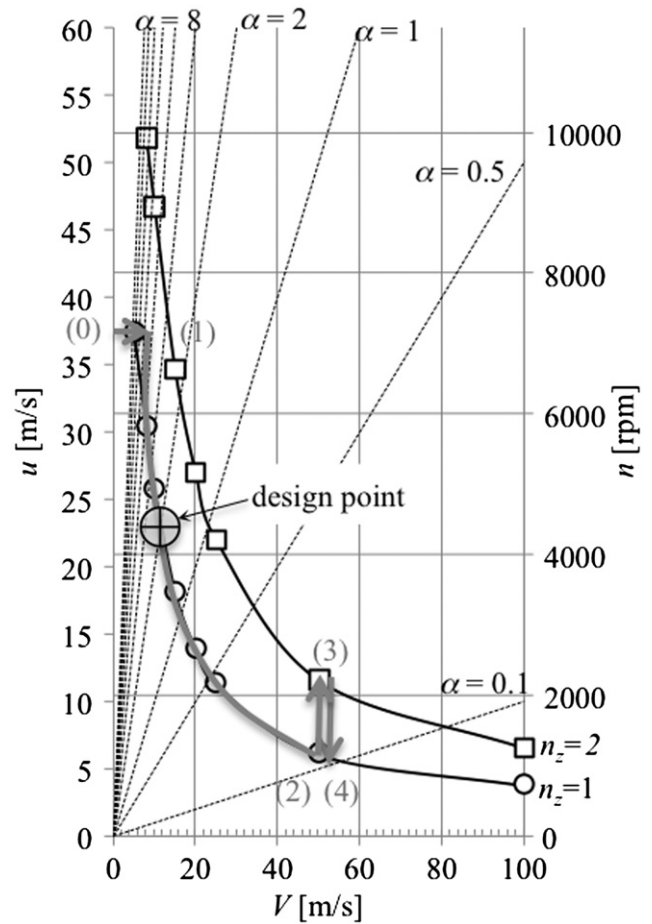


Fig. 59. Design Chart for the operating points of a Magnus rotor, developed by the author.

form of the lift curve and may be different at very large aspect ratios or with very large endplates. Aerodynamic efficiency, as determined by C_L/C_D , also quickly reaches a maximum and is not improved by further power input.

4.3. Stability and control of a rotor airplane

The only full-scale rotor airplane ever flown is the Plymouth A-A-2004 (see Fig. 36). Besides the unconventional rotating cylinders, this configuration had a conventional tail with control surfaces and a fuselage with a motor in the front. However, additional vertical control surfaces behind the motor and in front of the assumed center of gravity could have led to a destabilizing effect in lateral directional motion. The idea behind this unconventional solution was most likely the need for ailerons which could not be mounted to the cylinders. Another solution to control the roll motion could have been to turn the left and right cylinder at different speeds. Weissheimer [138] investigated an aileron in the flow behind the rotating cylinder. He provides information where to mount the control surfaces. However, the author's remote controlled flying model (Fig. 58) was controllable by a rudder only and provided sufficient stability within the tests performed.

The design and development of a future rotor airplane will have to include a proper flight control system, developed on the basis of an adequate flight mechanics model, to handle the gyroscopic forces as explained in Section 2.2.

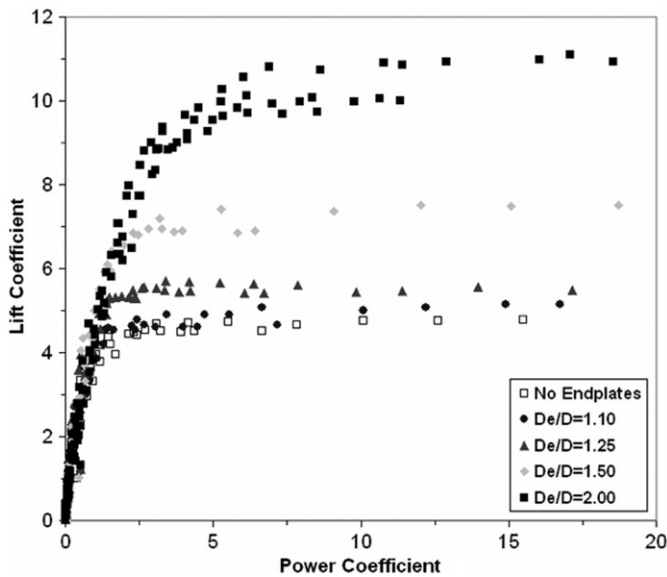


Fig. 60. Lift efficiency, reprinted from [55] with permission from AIAA.

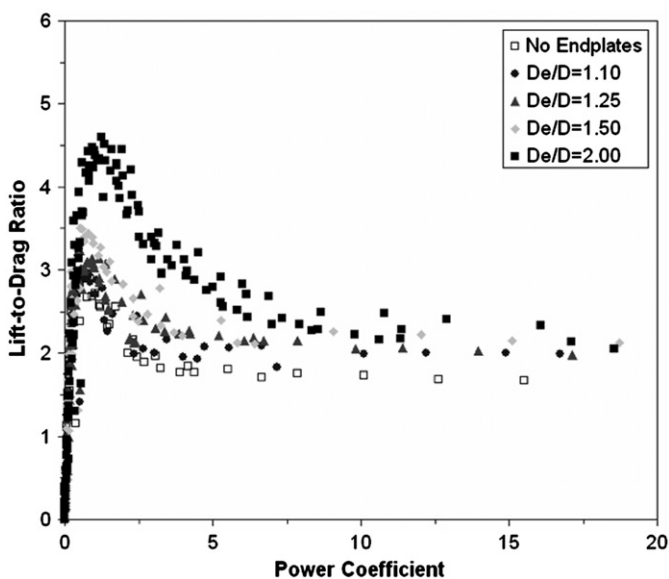


Fig. 61. Aerodynamic efficiency, reprinted from [55] with permission from AIAA.

5. Conclusions and outlook

This article attempted to provide the interested reader with a review of past and current Magnus effect research and development in aeronautics. The major advantages of a Magnus effect device are high-lift forces or rather high wing-loading and stall resistance. The disadvantages are the need for an additional driving mechanism with additional weight and complexity compared to a conventional wing. From a technical point of view, there are some mature Magnus effect devices available that can enhance the high-lift capability of a STOL aircraft or even the aerodynamic efficiency of a conventional aircraft, e.g., a wing with an integrated rotating cylinder. However, a comparison between alternative solutions on aircraft level is necessary, to estimate the benefits in terms of DOC and MRO.

One barrier for the application of Magnus rotors is the lack of design information, aerodynamic modeling and fundamentals of flight mechanics of rotor airplanes.

However, the Flettner-rotor, first applied in a rotor ship in the 1920s, is becoming again a hot topic as energy costs and climate change concerns are rising [139]. The new E-Ship1 of Enercon [140] is equipped with four Flettner-rotors, 27 m high and 4 m in diameter. A conventional cargo ship causes 4.5 million dollars in fuel cost a year (320 day of operation). E-Ship 1 is expected to reduce the costs by 30–40%. At 7 Beaufort, the main engines can be cut off and only the four Flettner-rotors are needed to bring the ship to maximum speed. The investment into the additional propulsion system will amortize in less than five years [141].

Many ideas exist on how to use the Magnus effect. Perhaps, Enercon's E-Ship may stimulate again the aeronautical community, as happened in the past.

Acknowledgements

The author gratefully acknowledges the help of all the people, who assisted to search in the archives of Deutsches Museum, Deutsches Schiffahrtsmuseum Bremerhaven, Smithsonian Institute, National Air and Space Museum Washington, the Public Library in Washington D.C. and Jane's. Some figures are reprinted by courtesy of Magenn Power Inc. and the American Institute of Aeronautics and Astronautics. Further material is used by permission of Koehler & Amelang. Finally, the author would like to acknowledge his gratitude to Mr. Dieter Schulz-Hoos and Dr. Andreas Sizmann for their interest in, and support of, the rotor airplane research.

Appendix A. Supplementary material

Supplementary data associated with this article can be found in the online version at <http://dx.doi.org/10.1016/j.paerosci.2012.07.001>.

References

- [1] Thomson JJ. The dynamics of a golf ball. *Nature* 1910;85(2147):251–7.
- [2] Newton I. Letter to Oldenburg. In: *Philosophical Transactions of the Royal Society* 1671. 7:3075–87.
- [3] Robins B. *New Principles of Gunnery*. London. 1805.
- [4] Tokaty GA. *A History and philosophie of fluid mechanics*. Dover: Dover Publications; 1994.
- [5] Magnus HG. Ueber die Abweichung der Geschosse, und; ueber eine auffallende Erscheinung bei rotirenden Körpern. Translated to: on the deviation of projectiles; and on a remarkable phenomenon of rotating bodies. *Taylor's Foreign Scientific Memoirs*, Berlin 1853:804–10.
- [6] Rayleigh L. On the irregular flight of a tennis ball. *Messenger of Mathematics* 1877;7:14.
- [7] Lafay A. Contribution expérimentale à l'aérodynamique du cylindre et à l'étude du phénomène de Magnus. *Revue de Méchanique* 1912;30:417–42.
- [8] Föttinger H. Neue Grundlagen für die theoretische und experimentelle Behandlung des Propellerproblems. *Jahrbuch der Schiffbautechnischen Gesellschaft*; 1918.
- [9] Gumbel. Modelle zur Versinnbildlichung der Wirbelgesetze. *Schiffbau* 1922:338–9.
- [10] Flettner A. *Mein Weg zum Rotor*. Leipzig: Koehler & Amelang. Translated to: the story of the Rotor. New York: published by F.O. Wilhoff; 1926.
- [11] Flettner A. Anwendung der Erkenntnisse der Aerodynamik zum Windvortrieb von Schiffen. *Zeitschrift für Flugtechnik und Motor-Luftschiffahrt* 1925;16(3):52–66.
- [12] Wagner CD. *Die Segelmaschine*. Hamburg: Kabel Verlag; 1991.
- [13] Reid ER. Tests of rotating cylinders. *NACA Technical Memorandum*. TM-209. 1924.
- [14] Thom A. *The aerodynamics of a rotating cylinder* [Dissertation]. Glasgow: University of Glasgow; 1926.
- [15] Thom A. Experiments on the flow past a rotating cylinder. *Aeronautical Research Committee, Reports and Memoranda* 1931;1410.
- [16] Thom A. Experiments on the air forces on rotating cylinders. *Aeronautical Research Committee, Reports and Memoranda* 1925;1018.

- [17] Thom A, Sengupta SR. Air torque on a cylinder rotating in an air stream. Aeronautical Research Committee, Reports and Memoranda 1932;1520.
- [18] Thom A. Effect of discs on the air forces on a rotating cylinder. Aeronautical Research Committee, Reports and Memoranda 1934;1623.
- [19] Thom A. The pressures round a cylinder rotating in an air current. Aeronautical Research Committee, Reports and Memoranda 1926;1082.
- [20] Swanson WM. The Magnus effect: a summary of investigations to date. *Journal of Basic Engineering Transactions of ASME* 1961;83(3):470.
- [21] Calderon AA, Arnold FR. A study of the aerodynamic characteristics of a high-lift device based on a rotating cylinder and flap [Technical Report RCF-1]. Stanford University; 1961.
- [22] Cichy DR, Harris JW, Mackay JK. Flight tests of a rotating cylinder flap on a North American Rockwell YOY-10 aircraft. NASA. CR-2135. 1972.
- [23] Iversen JD. Correlation of Magnus force data for slender spinning cylinders. *Journal of Spacecraft and Rockets* 1973;10(4):268–72. <http://dx.doi.org/10.2514/3.61877>.
- [24] Borg J. Magnus effect: an overview of its past and future practical applications 1986;1 and 2 AD-A 165 902. NAVY NSSCDot.
- [25] Zdravkovich MM. Flow around circular cylinders. Vol. 1: fundamentals. New York: Oxford University Press, Inc; 1997.
- [26] Zdravkovich MM. Flow around circular cylinders. Vol. 2: applications. New York: Oxford University Press, Inc; 2003.
- [27] Rizzo F. The Flettner rotor ship in the light of the Kutta–Joukowski theory and of experimental results. TM-228. NACA Technical Memorandum; 1925.
- [28] Prandtl L. Über Flüssigkeitsbewegung bei sehr kleiner Reibung. In: *Proceedings of Dritter Internationaler Mathematiker Kongress*. Heidelberg. 1904:484–491.
- [29] Ahlborn F. Der Magnuseffekt in Theorie und Wirklichkeit. *Zeitschrift für Flugtechnik und Motorluftschiffahrt*. Translated to: the Magnus effect in theory and in reality. NACA Technical Memorandum 1929;TM-567:642–53.
- [30] Ericsson LE. Moving wall effects in unsteady flow. *Journal of Aircraft* 1988;25(11):977–90.
- [31] Relf EF, Lavender T. Experiments on the flow behind a rotating cylinder in the water channel. Aeronautical Research Committee, Reports and Memoranda 1925;1009.
- [32] Prandtl L. Kinematographische Strömungsbilder. Die Naturwissenschaften. Translated to: Kinetographic flow pictures. NACA Technical Memorandum 1926;TM-364:1050–3.
- [33] Bickley WG. The influence of vortices upon the resistance experienced by solids moving through a liquid. In: *Proceedings of Royal Society of London*. London. 1928;119:146–156. <http://dx.doi.org/10.1098/rspa.1928.0089>.
- [34] The rotor airship. *Modern Mechanix*. 1931. p. 59.
- [35] Deumig K. *Illustrierte Technik*. Das Industrieblatt Stuttgart.
- [36] Flettner A. Arrangement for exchanging energy between a current and a body therein. U. S. Patent, 1,674,169. 1928.
- [37] Stiotta HH. Der Rotorplan. *Motor und Sport* 1925;2(31):22–3.
- [38] Flettner A. Verfahren zur Erzeugung des Quertriebes an Quertriebskörpern. Patentschrift: z. B. an Segeln von Schiffen; 1923 DE420840.
- [39] Thouault N, Breitsamter C, Adams NA. Numerical analysis of a rotating cylinder with spanwise discs. Annual Report for Bauhaus Luftfahrt. 2009.
- [40] Mittal S, Kumar B. Flow past a rotating cylinder. *Journal of Fluid Mechanics* 2003;476:303–34. <http://dx.doi.org/10.1017/S0022112002002938>.
- [41] Badalamenti C, Prince SA. Vortex shedding from a rotating circular cylinder at moderate sub-critical Reynolds numbers and high velocity ratio. 26th International Congress of the Aeronautical Sciences Anchorage. 2008.
- [42] Diaz F, Gavalda J, Kawall JG, Keffer JF, Giral F. Vortex shedding from a spinning cylinder. *Physics of Fluids* 1983;26(12):3460. <http://dx.doi.org/10.1063/1.864127>.
- [43] Tanaka H, Nagano S. Study of flow around a rotating circular cylinder. *Bulletins of the Japanese Society of Mechanical Engineers* 1973;16(92):234–43.
- [44] Lafay A. Sure l'Inversion de Phenomene de Magnus. *Comptes Rendus* 1910:151.
- [45] Ericsson LE, Beyers ME. Universality of the moving-wall effect. *Journal of Aircraft* 2000;37(3):508–13. <http://dx.doi.org/10.2514/2.2627>.
- [46] Ericsson LE. Moving wall effect in relation to other dynamic stall flow mechanisms. *Journal of Aircraft* 1994;31(6):1303–9. <http://dx.doi.org/10.2514/3.46651>.
- [47] Fletcher CAJ. Negative Magnus forces in the critical Reynolds number regime. *Journal of Aircraft* 1972;9(12):826–34. <http://dx.doi.org/10.2514/3.44343>.
- [48] Krahn E. Negative Magnus force. *Journal of Aeronautical Sciences* 1956;23(4):377–8.
- [49] Lugt HJ. Autorotation. *Annual Review of Fluid Mechanics* 1983;15:123–47.
- [50] Iversen JD. The Magnus rotor as an aerodynamic decelerator. Aerodynamic deceleration systems conference. AIAA. El Centro. 1968.
- [51] Miller MC. Wind-tunnel measurements of the surface pressure distribution on a spinning Magnus rotor. *Journal of Aircraft* 1979;16(12):815–22. <http://dx.doi.org/10.2514/3.58609>.
- [52] Zaic F. *Modell aeronautics year book*. Model Aeronautic Publications; 1965.
- [53] Salter SH. Aerodynamics in a spin. *Nature* 1991;352:470–1. <http://dx.doi.org/10.1038/352470a0>.
- [54] Skewes BW. Autorotation of many-sided bodies in an airstream. *Nature* 1991;352:512–3. <http://dx.doi.org/10.1038/352512a0>.
- [55] Badalamenti C, Prince S. Effects of endplates on a rotating cylinder in crossflow. 26th AIAA applied aerodynamics conference. AIAA. Honolulu, Hawaii. 2008.
- [56] Hoffman J, Johnson C. Computational turbulent incompressible flow. Springer; 2007.
- [57] Luo SC, Lua KB, Goh EKR. Side force on an ogive cylinder: effects of surface roughness. *Journal of Aircraft* 2002;39(4):716–8.
- [58] Modi VJ, Munshi SR, Bandyopadhyay G, Yokomizo T. High-performance airfoil with moving surface boundary-layer control. *Journal of Aircraft* 1998;35(4):553. <http://dx.doi.org/10.2514/2.2358>.
- [59] Swanson WM. An experimental investigation of the Magnus effect. Case Institute of Technology. Final report. 1956.
- [60] Prandtl L. Magnuseffekt und Windkraftschiff. Die Naturwissenschaften. Translated to: application of the “Magnus Effect” to the wind propulsion of ships. NACA Technical Memorandum 1925;TM-367:93–108.
- [61] Ackeret J. Neuere Untersuchungen der Aerodynamischen Versuchsanstalt, Göttingen. *Zeitschrift für Flugtechnik und Motorluftschiffahrt* 1925;16(3):52.
- [62] Busemann A. Messungen an Rotierenden Zylindern. In: Prandtl L, Betz A, editors. *Ergebnisse der Aerodynamischen Versuchsanstalt zu Göttingen*. IV. München: R. Oldenbourg; 1932. p. 101–6 Lieferung.
- [63] Thouault N, Breitsamter C, Seifert J, Badalamenti C, Prince SA, Adams NA. Numerical analysis of a rotating cylinder with spanwise discs. Nizza: International Congress of the Aeronautical Sciences; 2010.
- [64] Norwood J. 21st century multihulls-rotors. *Amateur Yacht Research Society*; 1995 120-II:21.
- [65] Ackeret J. Neuere Untersuchungen der Aerodynamischen Versuchsanstalt, Göttingen. *Zeitschrift für Flugtechnik und Motorluftschiffahrt*. Translated to: recent experiments at the Göttingen aerodynamic institute. NACA Technical Memorandum TM-323. 1925. p. 44–52.
- [66] Betz A. Der Magnuseffekt, die Grundlage der Flettner—Walze. *Zeitschrift des vereins deutscher Ingenieure*. Translated to: the “Magnus Effect”. The Principle of the Flettner rotor. NACA Technical Memorandum 1925;TM-310:9–14.
- [67] Abbott IH, Doenhoff von AE. *Theory of wing sections: including a summary of airfoil data*. Dover Publ Inc; 1960.
- [68] Leishman JG. Development of the autogiro: a technical perspective. *Journal of Aircraft* 2004;41(4):765–81. <http://dx.doi.org/10.2514/1.1205>.
- [69] Potts JR, Crowther WJ. Flight control of a spin stabilised axis-symmetric disc-wing. In: *Proceedings of AIAA aerospace sciences meeting*. Reno. 2001:10.
- [70] Gress GR. Lift fans as gyroscopes for controlling compact VTOL air vehicles: overview and development status of oblique active tilting. *American Helicopter Society 63rd Annual Forum*. American Helicopter Society International. Virginia Beach; 2007.
- [71] Rotor ships B L. *Nature* 1924;114(2873):758.
- [72] The flettner rotor ship: is the principle applicable to aircraft? *Flight—aircraft engineer and airships* 1924:741.
- [73] *New Aircraft*. The Evening Sun. 23. July 1910.
- [74] NavSource Naval History: Yarnall PR. Internet: <<http://www.navsource.org/archives/05/tb/050324.htm>>; (accessed on: 10/05/2010).
- [75] Aerofiles: Eckland KO. Internet: <http://www.aerofiles.com/_al_html>; (accessed on: 10/05/2010).
- [76] Spooner S. The rotor and aviation. *Flight—Aircraft Engineer and Airships* 1924. November, 27th. p. 739–40.
- [77] Kieran LA. Rotor plane may open new vista to aircraft. *The New York Times*; 1930 24. August, p. 5.
- [78] Latest in flying ships—plane without wings. *The Washington Times*. 21. August 1930.
- [79] Whirling spoils lift this plane. *Popular science monthly*. 5 1930. November. p. 162.
- [80] Rotor-flugzeug. *Technik für Alle*. 1932.
- [81] Lee RK, Zaparka EF. Propeller. U. S. Patent, 1,977,681. 1932.
- [82] Zaparka EF. Aircraft. U. S. Patent, 1,927,535. 1929.
- [83] Zaparka EF. Aircraft sustaining system and propulsion. U. S. Patent, 1,927,536. 1929.
- [84] Zaparka EF. Aircraft control. U. S. Patent, 1,927,537. 1929.
- [85] Zaparka EF. Sustaining and control surface. U. S. Patent, 1,927,538. 1930.
- [86] Zaparka EF. Aircraft. U. S. Patent, 2,039,676. 1930.
- [87] Smithsonian Institution NAD. Historical aircraft listing. Washington. 2002.
- [88] Chappedelaine JLMO. Aeroplane with rotatable wings. United Kingdom Patent, GB402922A. 1933.
- [89] Calderon AA. Rotating cylinder flaps for V/S.T.O.L aircraft: some aspects of an investigation into the rotating cylinder flap high lift system for V/S.T.O.L. Aircraft conducted jointly by the Peruvian Air Force and The National University of Engineering of Peru. *Aircraft Engineering and Aerospace Technology* 1964;36(10):309. <http://dx.doi.org/10.1108/eb033937>.
- [90] Weiberg JA, Gamse B. Large-scale wind-tunnel tests of an airplane model with two propellers and rotating cylinder flaps. *NASA Technical Note*. TN-D-4489. 1968.
- [91] Weiberg JA, Dickinson SO. Large-scale wind-tunnel tests of an airplane model with four propellers and rotating cylinder flaps. *NASA Technical Note*. TN-D-5742. 1970.
- [92] Cook WL, Hickey DH. Correlation of low speed wind tunnel and flight test data for V/STOL aircraft, TM X-62423. NASA Ames Research Center; 1975.
- [93] Weiberg JA, Giulianetti D, Gambucci B, Innis RC. Takeoff and landing performance and noise characteristics of a deflected slipstream STOL airplane with interconnected propellers and rotating cylinder flaps. *NASA Technical Memorandum*. TM-X-62320. 1973.

- [94] Wolff EB. Preliminary investigation of the effect of a rotating cylinder in a wing. NACA Technical Memorandum. TM-307. 1925.
- [95] Wolff EB, Koning C. Tests for determining the effect of a rotating cylinder fitted into the leading edge of an airplane wing NACA Technical Memorandum. TM-354. 1926.
- [96] Tennant JS, Johnson WS, Krothapalli A. Rotating cylinder for circulation control on an airfoil. *Journal of Hydronautics* 1976;10(3):105, <http://dx.doi.org/10.2514/3.48147>.
- [97] Tennant JS, Johnson WS, Keaton DD. On the calculation of boundary layers along rotating cylinders. *Journal of Hydronautics* 1977;11(2):63, <http://dx.doi.org/10.2514/3.48154>.
- [98] Tennant JS, Johnson WS, Keaton DD. Boundary-layer flows from fixed to moving surfaces including gap effects. *Journal of Hydronautics* 1978;12(2):84, <http://dx.doi.org/10.2514/3.48161>.
- [99] Al-Garni AZ, Al-Garni AM, Ahmed SA, Sahin AZ. Flow control for an airfoil with leading-edge rotation: an experimental study. *Journal of Aircraft* 2000;37(4):622, <http://dx.doi.org/10.2514/2.2673>.
- [100] Al-Garni AZ, Al-Qutub AM. Movable surface plane. Patent, US 6,622,973 B2. 2003.
- [101] Mokhtarian F, Modi VJ. Fluid dynamics of airfoils with moving surface boundary-layer control. *Journal of Aircraft* 1988;25(2):169, <http://dx.doi.org/10.2514/3.45557>.
- [102] Modi VJ, Mokhtarian F, Fernando MS, Yokomizo T. Moving surface boundary-layer control as applied to two-dimensional airfoils. *Journal of Aircraft* 1991;28(2):112, <http://dx.doi.org/10.2514/3.45998>.
- [103] Modi VJ. Moving surface boundary-layer control: a review. *Journal of Fluid Structure* 1997;11(6):663, <http://dx.doi.org/10.1006/jfls.1997.0098>.
- [104] Modi VJ, Fernando MS, Yokomizo T. Moving surface boundary-layer control: studies with bluff bodies. *AIAA Journal* 1991;29(9):1406, <http://dx.doi.org/10.2514/3.10753>.
- [105] Modi VJ, Mokhtarian F, Yokomizo T. Effect of moving surfaces on the airfoil boundary-layer control. *Journal of Aircraft* 1990;27(1):50, <http://dx.doi.org/10.2514/3.45894>.
- [106] Modi VJ, Sun JLC, Akutsu T, Lake P, McMillan K, Swinton PG, et al. Moving-surface boundary-layer control for aircraft operation at high incidence. *Journal of Aircraft* 1981;18(11):968, <http://dx.doi.org/10.2514/3.57587>.
- [107] Mokhtarian F, Modi VJ, Yokomizo T. Rotating air scoop as airfoil boundary-layer control. *Journal of Aircraft* 1988;25(10):975, <http://dx.doi.org/10.2514/3.45689>.
- [108] Du X, Lee T, Mokhtarian F, Kafyeke F. Flow past an airfoil with a leading-edge rotation cylinder. *Journal of Aircraft* 2002;39(6):1084, <http://dx.doi.org/10.2514/2.3040>.
- [109] Tennant JS, Yang T. Turbulent boundary-layer flow from stationary to moving surfaces. *AIAA Journal* 1973;11(8):1160, <http://dx.doi.org/10.2514/3.6887>.
- [110] Tennant JS. A subsonic diffuser with moving walls for boundary-layer control. *AIAA Journal* 1973;11(2):242, <http://dx.doi.org/10.2514/3.6735>.
- [111] Buerge BT. The vortex flap: an experimental investigation into the use of external rotating cylinders for lift augmentation In: *Proceedings of international powered lift conference*. London. 2009.
- [112] Seifert J. Aerodynamic analysis of a new hybrid rotor. In: *Proceedings of Deutscher Luft- und Raumfahrt Kongress*. Aachen. 2009:7.
- [113] Seifert J. Fluggerät mit rotierenden Zylindern zur Erzeugung von Auftrieb und/oder Vortrieb. translation: Aircraft with rotating cylinders to generate lift and/or thrust. German patent, DE102007009951B3. 2008.
- [114] Kirsten FK. Cycloidal propulsion applied to aircraft. In: *Proceedings of first national meeting of the ASME aeronautics division*. Detroit. 1928.
- [115] Wheatley JB. Simplified aerodynamic analysis of the cyclogiro rotating-wing system. NACA Technical Note. No. 467. Laboratory LMA; 1933.
- [116] Wheatley JB, Windler R. Wind-tunnel tests of a cyclogiro rotor. NACA Technical Note. No. 528. Laboratory LMA; 1935.
- [117] Gibbens RP. The cycloidal propeller for twenty first century airships. In: *Proceedings of AIAA lighter-than-air systems technology conference*. San Diego. 1991:101–105.
- [118] Boshma JH. Cycloidal propulsion for UAV VTOL applications. Final report for Government Technical Liaison Naval Air Warfare Center—Aircraft Division. 1998.
- [119] Gibbens RP, Boshma JH, Sullivan C. Construction and testing of a new aircraft cycloidal propeller In: *Proceedings of AIAA lighter-than-air systems technology conference*. Norfolk. 1999:132–140.
- [120] Boshma JH. Modern aviation applications for cycloidal propulsion. AIAA aircraft, Technology integration, and operations forum. Los Angeles: AIAA; 2001 1–6.
- [121] Iosilevskii G, Levy Y. Aerodynamics of the cyclogiro. 33rd AIAA fluid dynamics conference and exhibit. AIAA. Orlando. 2003:1–9.
- [122] Kim S, Yun C, Kim D, Yoon Y, Park I. Design and performance tests of cycloidal propulsion systems. 44th AIAA/ASME/ASCE/AHS/ASC structures, structural dynamics, and materials conference. Norfolk. 2003.
- [123] Yun CY, Park I, Lee HY, Junng JS, Hwang IS, Kim SJ, et al. A new VTOL UAV cyclocopter with cycloidal blades system. *American helicopter society 60th annual forum*. Baltimore. 2004.
- [124] Hwang IS, Min SY, Kim MK, Kim SJ. Multidisciplinary optimal design of cyclocopter blade system 46th AIAA/ASME/ASCE/AHS/ASC structures, structural dynamics and materials conference. AIAA. Austin, Texas. 2005:1–7.
- [125] Hwang IS, Hwang CS, Kim SJ. Structural design of cyclocopter blade system In: *Proceedings of 46th AIAA/ASME/ASCE/AHS/ASC structures, structural dynamics and materials conference*. Austin, Texas. 2005.
- [126] Parsons E. Investigation and characterization of a cycloidal rotor for application to a micro air vehicle [Master thesis]: University of Maryland. Department of Aerospace Engineering; 2005.
- [127] Yun CY, Park IK. Thrust control mechanism of VTOL UAV cyclocopter with cycloidal blades system. *Journal of Intelligent Material Systems and Structures* 2005;16(11):937–43, <http://dx.doi.org/10.1177/1045389x05057520>.
- [128] Hwang IS, Hwang CS, Min SY, Jeong IO, Lee CH, Lee YH, et al. Design and testing of VTOL UAV cyclocopter with 4 rotors. *American helicopter society 62nd annual forum*. American helicopter society international. Arizona: Phoenix; 2006.
- [129] Iosilevskii G, Levy Y. Experimental and numerical study of cyclogiro aerodynamics. *AIAA Journal* 2006;44(12):2866–70, <http://dx.doi.org/10.2514/1.8227>.
- [130] Yu H, Bin LK, Beng TW. The investigation of cyclogiro design and the performance. 25th international congress of the aeronautical sciences. Hamburg. 2006.
- [131] Yu H, Beng TW, Bin LK. The analysis of cyclogiro using unsteady vortex lattice method. 25th international congress of the aeronautical sciences. Hamburg. 2006.
- [132] Hwang IS, Min SY, Lee CH, Kim SJ. Experimental investigation of VTOL UAV cyclocopter with four rotors. 48th AIAA/ASME/ASCE/AHS/ASC structures, structural dynamics and materials conference. AIAA. Honolulu, Hawaii. 2007.
- [133] Hwang IS, Min SY, Lee CH, Kim SJ. Development of a four-rotor cyclocopter. *Journal of Aircraft* 2008;45(6):2151–7, <http://dx.doi.org/10.2514/1.35575>.
- [134] Johnson RF. Those magnificent men and their hybrid rotor. Berlin: Aviation Week ShowNews ILA; 2010.
- [135] Marchman JF, Abtahi AA. Aerodynamics of an aspect ratio 8 wing at low Reynolds numbers. *Journal of Aircraft* 1985;22(7):628–34, <http://dx.doi.org/10.2514/3.45176>.
- [136] Testing the Flettner "Rotor" in actual flight. *Flight—Aircraft Engineer and airships* 1924. December, 4th. p. 759.
- [137] Seifert J. Resistenz eines Rotorflugzeugs gegenüber Turbulenz. Translated to: insensitivity of a rotor airplane against gust (unpublished). 2010.
- [138] Weissheimer FW. Flugzeug, WO 89/07073. 1989.
- [139] Reuß H-J. Flettner-Rotorschiffe—Alte Technik für neue Schiffe. *International Maritime Journal* 2007;144(12):16–22.
- [140] Powered by sailing rotors: E-Ship 1 in the testing phase. *Windblatt*. 02 2010. p. 06–07.
- [141] Köpke R. Mit rotierenden Säulen über die Meere. *Berliner Zeitung*. 09. Nov. 2006.